Chaos: A Tutorial for Engineers

THOMAS S. PARKER AND LEON O. CHUA, FELLOW, IEEE

Invited Paper

This tutorial presents an in-depth introduction to chaos in dynamical systems, and presents several practical techniques for recognizing and classifying chaotic behavior. These techniques include the Poincaré map, Lyapunov exponents, capacity, information dimension, correlation dimension, Lyapunov dimension, and the reconstruction of attractors from a single time series.

I. Introduction

Nonlinear systems have always played an important role in the study of natural phenomena, but the last decade has seen a heightened interest and renewed vigor in nonlinear systems research.

The main reason for this growth is the recent availability of inexpensive computing power. Unlike linear systems where knowledge of the eigenvalues and eigenvectors allows one to write a closed-form solution, few nonlinear systems possess closed-form solutions and, therefore, numerical simulations play a crucial role in the process of finding and analyzing nonlinear phenomena. Before the advent of low-cost computers, the ability to perform nonlinear simulations was restricted to researchers with access to a large computing facility; now, anyone with a personal computer may simulate a nonlinear system.

The increased interest in nonlinear systems is also due to the recent (within the last fifteen years) discovery of chaos. One of the basic tenets of science is that deterministic systems are predictable: given the initial condition and the equations describing a system, the behavior of the system can be predicted for all time.[1] The discovery of chaotic systems has eliminated this viewpoint. Simply put, a chaotic system is a *deterministic* system that exhibits *random* behavior. Chaos, also called *strange behavior*, is currently one of the most exciting topics in nonlinear systems research.

The purpose of this tutorial is two-fold. We will explain how a deterministic system can be unpredictable, and we will present several practical methods for categorizing the steady-state behavior of nonlinear systems with an emphasis on classifying strange behavior.

This tutorial is divided into two parts. Part I presents the theoretical basis of the analysis methods while Part II outlines practical numerical algoirthms to implement them.

The field of chaotic dynamics is rapidly growing. Two general, up-to-date references are [1] which is in the spirit of this tutorial and [2] which takes a more mathematical approach.

Manuscript received December 15, 1986; revised May 19, 1987. This research was supported in part by the Hertz Foundation, by the Office of Naval Research under Contract N00014-86-K-0351, and by the National Science Foundation under Grant MIP-8614000.

The authors are with the Department of Electrical Engineering and Computer Science, University of California, Berkeley, CA 94720, USA.

IEEE Log Number 8715760.

[1]There are random events in nature, but science has typically used *probabilistic* models to describe them.

Part I: Theoretical Aspects

II. Dynamical Systems

In this section, we define three types of dynamical systems and present some useful facts from the theory of differential equations.

A. Autonomous Dynamical Systems

An *nth-order autonomous dynamical system* is defined by the state equation

$$\dot{x} = f(x) \qquad x(t_0) = x_0 \tag{1}$$

where $\dot{x} := dx/dt$, $x(t) \in \mathbb{R}^n$ is the state at time t and $f: \mathbb{R}^n \to \mathbb{R}^n$ is called the vector field. Since the vector field does not depend on time, the initial time may always be taken as $t_0 = 0$. The solution to (1) with initial condition x_0 at time $t = 0$ is called a *trajectory* and is denoted by $\phi_t(x_0)$. The mapping $\phi_t: \mathbb{R}^n \to \mathbb{R}^n$ is called the *flow* of the system. The dynamical system (1) is linear if $f(x)$ is linear.

B. Nonautonomous Dynamical Systems

An *nth-order nonautonomous dynamical system* is defined by the time-varying state equation

$$\dot{x} = f(x, t) \qquad x(t_0) = x_0. \tag{2}$$

The vector field f depends on time and, unlike the autonomous case, the initial time cannot arbitrarily be set to 0. The solution to (2) passing through x_0 at time t_0 is $\phi_t(x_0, t_0)$. The system is linear if f is linear with respect to x.

0018-9219/87/0800-0982$01.00 © 1987 IEEE

If there exists a $T > 0$ such that $f(x, t) = f(x, t + T)$ for all x and all t, the system is said to be *time-periodic* with period T. The smallest such T is called the *minimal period*. In this tutorial, all nonautonomous systems are assumed to be time-periodic.

An nth-order time-periodic nonautonomous system can always be converted to an $(n + 1)$th-order autonomous system by appending an extra state $\theta := 2\pi t/T$. The autonomous system is given by

$$\dot{x} = f(x, \theta T/2\pi) \qquad x(0) = x_0$$
$$\dot{\theta} = 2\pi/T \qquad \theta(0) = 2\pi t_0/T. \tag{3}$$

Since f is time-periodic with period T, the new system (3) is periodic in θ with period 2π. Hence, the planes $\theta = 0$ and $\theta = 2\pi$ can be identified and the state space transformed from the Euclidean space $\mathbb{R}^{n+1}$ to the cylindrical state space $\mathbb{R}^n \times S$ where $S := [0, 2\pi)$ is the circle. The solution in the new state space is

$$\begin{bmatrix} x(t) \\ \theta(t) \end{bmatrix} = \begin{bmatrix} \phi_t(x_0, t_0) \\ \dfrac{2\pi t}{T} \bmod 2\pi \end{bmatrix} \tag{4}$$

where the modulo function[2] restricts $0 \le \theta < 2\pi$. Using this transformation, results for autonomous systems can be applied to the time-periodic nonautonomous case.[3]

C. Useful Facts About Dynamical Systems

There are several standard and useful facts concerning the existence and uniqueness of solutions to dynamical systems. Precise statements of these theorems can be found in any text on differential equations (e.g., [3]).

For this tutorial, we assume that for any finite t, ϕ_t is a diffeomorphism.[4] This is not a restrictive assumption and has several consequences:

i) $\phi_t(x) = \phi_t(y)$ if and only if $x = y$. Hence, trajectories of autonomous systems are uniquely specified by their initial condition.

ii) $\phi_t(x, t_0) = \phi_t(y, t_0)$ if and only if $x = y$. This implies that given the initial time, a trajectory of a nonautonomous system is uniquely specified by the initial state; however, if $t_0 \neq t_1$, it is possible that $\phi_t(x, t_0) = \phi_t(y, t_1)$ and $x \neq y$ showing that, unlike autonomous systems, the trajectories of nonautonomous systems can intersect.

iii) The derivative of a trajectory with respect to the initial condition exists and is nonsingular. It follows that for t and t_0 fixed, $\phi_t(x_0, t_0)$ is continuous with respect to the initial condition.

D. Discrete-Time Dynamical Systems

Any map $f: \mathbb{R}^n \to \mathbb{R}^n$ defines a discrete-time dynamical system by the state equation

$$x_{k+1} = f(x_k), \qquad k = 0, 1, 2, \cdots \tag{5}$$

where $x_k \in \mathbb{R}^n$ is called the state, and f maps the state x_k to the next state x_{k+1}. Starting with an initial condition x_0, repeated applications of the map f give rise to a sequence of points $\{x_k\}_{k=0}^{\infty}$ called an *orbit* of the discrete-time system.

Although this tutorial focuses on continuous-time dynamical systems, discrete-time systems will be useful for two reasons. First, the Poincaré map—a technique that replaces the analysis of the flow of a continuous-time system with the analysis of a discrete-time system—is an extremely useful tool for studying dynamical systems. Second, due to this correspondence between flows and maps, maps will be used to illustrate important concepts without getting bogged down in the details of solving differential equations.

III. Steady-State Behavior and Limit Sets

In this section, dynamical systems are classified in terms of their steady-state solutions and limit sets. We start with some definitions.

Steady-state refers to the asymptotic behavior as $t \to \infty$. It is required that the steady state be bounded. The difference between the solution and its steady state is called the *transient*.

A point y is a *limit point* of x if, for every neighborhood U of y, $\phi_t(x)$ repeatedly enters U as $t \to \infty$.

The set of all limit points of x is called the *limit set* $L(x)$ of x. Limit sets are closed and invariant[5] under ϕ_t.

A limit set L is *attracting* if there exists an open neighborhood U of L such that $L(x) = L$ for all $x \in U$.

The *basin of attraction* $B(L)$ of an attracting set L is defined as the union of all such neighborhoods U. Every trajectory starting in $B(L)$ tends toward L as $t \to \infty$.

Attracting limit sets are of special interest since nonattracting limit sets cannot be observed in physical systems or simulations.[6]

Limit sets are useful for categorizing the classical types of steady-state behavior (e.g., equilibrium points, limit cycles), but the definition is too simple for the complex steady-state behavior found in chaotic systems. Historically, the term *strange attractor* has been used to describe the object on which the trajectories of a chaotic system accumulate; however, the question of how best to define an attractor is an open one [4]. For the purposes of this tutorial, the terms *attracting limit set* and *attractor* will be used interchangeably.

In a stable linear system, there is only one limit set. Hence, the steady-state behavior is independent of the initial condition and it makes sense to speak, for example, of *the* sinusoidal steady state. In a typical nonlinear system, however, there can be several limit sets. In particular, there can be several attracting limit sets, each with a different basin of attraction. The initial condition determines in which limit set the system eventually settles.

Four different types of steady-state behavior will now be presented starting with the simplest and moving to the most complex. Each steady state will be described from three dif-

[2] $u \bmod v$, gives the remainder of u divided by v, e.g., $5 \bmod 3 = 2$.

[3] A nonautonomous system that is not time-periodic can also be converted to an autonomous system using (3) with any $T > 0$; however, the solution will necessarily be unbounded ($\theta \to \infty$ as $t \to \infty$) and many of the results from autonomous theory about asymptotic behavior will not apply.

[4] A function of f is a *diffeomorphism* if f^{-1} exists and both Df and Df^{-1} exist and are continuous.

[5] A set L is *invariant* under ϕ_t if, for all $x \in L$ and all t, $\phi_t(x) \in L$.

[6] Note, however, that nonattracting limit sets can have a profound influence on the transient behavior of the system.

Fig. 1. Phase portrait of the pendulum equation. The white trajectories have been randomly chosen to indicate typical behavior of the system. There are two stable equilibria at $(\pm\pi, 0)$ and three saddle points at $(0, 0)$ and $\$(\pm 2\pi, 0)\$$. Each red trajectory tends toward one of the saddle points as $\$t \to \infty$ or as $t \to -\infty$. Each of the two shaded regions indicates the basin of attraction of one of the stable equilibria. Note that the red trajectories that approach the saddle points as $t \to \infty$ are the boundaries of the basins of attraction.

ferent points of view: in the time domain, in the frequency domain, and as a limit set (state-space domain).

A. Equilibrium Points

An equilibrium point x_{eq} of an autonomous system[7] is a constant solution of (1), $\phi_t(x_{eq}) = x_{eq}$ for all t. At an equilibrium point, the vector field vanishes and, except for a few pathological cases [5], $f(x) = 0$ implies that x is an equilibrium point.

A simple example is the damped pendulum equation

$$\begin{aligned} \dot{x} &= y \\ \dot{y} &= -ky - \sin x \end{aligned} \tag{6}$$

which is a second-order autonomous system with an infinity of equilibrium points at $(x, y) = (k\pi, 0)$, $k = 0, \pm 1, \pm 2, \cdots$. Some of the equilibrium points and their basins of attraction are shown in Fig. 1.

The limit set for an equilibrium point is just the equilibrium point itself.

B. Periodic Solutions

$\phi_t(x^*, t_0)$ is a *periodic solution* if

$$\phi_t(x^*, t_0) = \phi_{t+T'}(x^*, t_0) \tag{7}$$

for all t and some minimal period $T' > 0$.

A periodic solution has a Fourier transform consisting of a fundamental component at $f = 1/T'$ and evenly spaced harmonics at k/T', $k = 2, 3, \cdots$. The amplitude of some of these spectral components may be zero.

In a nonautonomous system, T' is typically some multiple, $K = 1, 2, \cdots$, of the forcing period T, and the solution is called a *period-K* solution. If $K \geq 2$, the solution is also referred to as a *Kth-order subharmonic*. For an asymptotically stable linear system, the sinusoidal steady state is a period-one solution and subharmonics cannot occur. Fig. 2 shows fundamental and subharmonic solutions together with their Fourier transforms for Duffing's equation

$$\begin{aligned} \dot{x} &= y \\ \dot{y} &= x - x^3 - \delta y + \gamma \cos \omega t. \end{aligned} \tag{8}$$

In the autonomous case, an isolated[8] periodic solution $\phi_t(x^*)$ is called a *limit cycle*. A limit cycle is a self-sustained oscillation and cannot occur in a linear system.

The classic example of a limit cycle is found in van der Pol's equation

$$\begin{aligned} \dot{x} &= y \\ \dot{y} &= (1 - x^2)y - x. \end{aligned} \tag{9}$$

The existence of the van der Pol limit cycle, shown in Fig. 3, may be explained by casting (9) into a scalar differential equation

$$\ddot{x} + (x^2 - 1)\dot{x} + x = 0. \tag{10}$$

[7]A nonautonomous system typically does not have equilibrium points because the vector field varies with time.

[8]A periodic solution is *isolated* if there exists a neighborhood of it that contains no other periodic solutions.

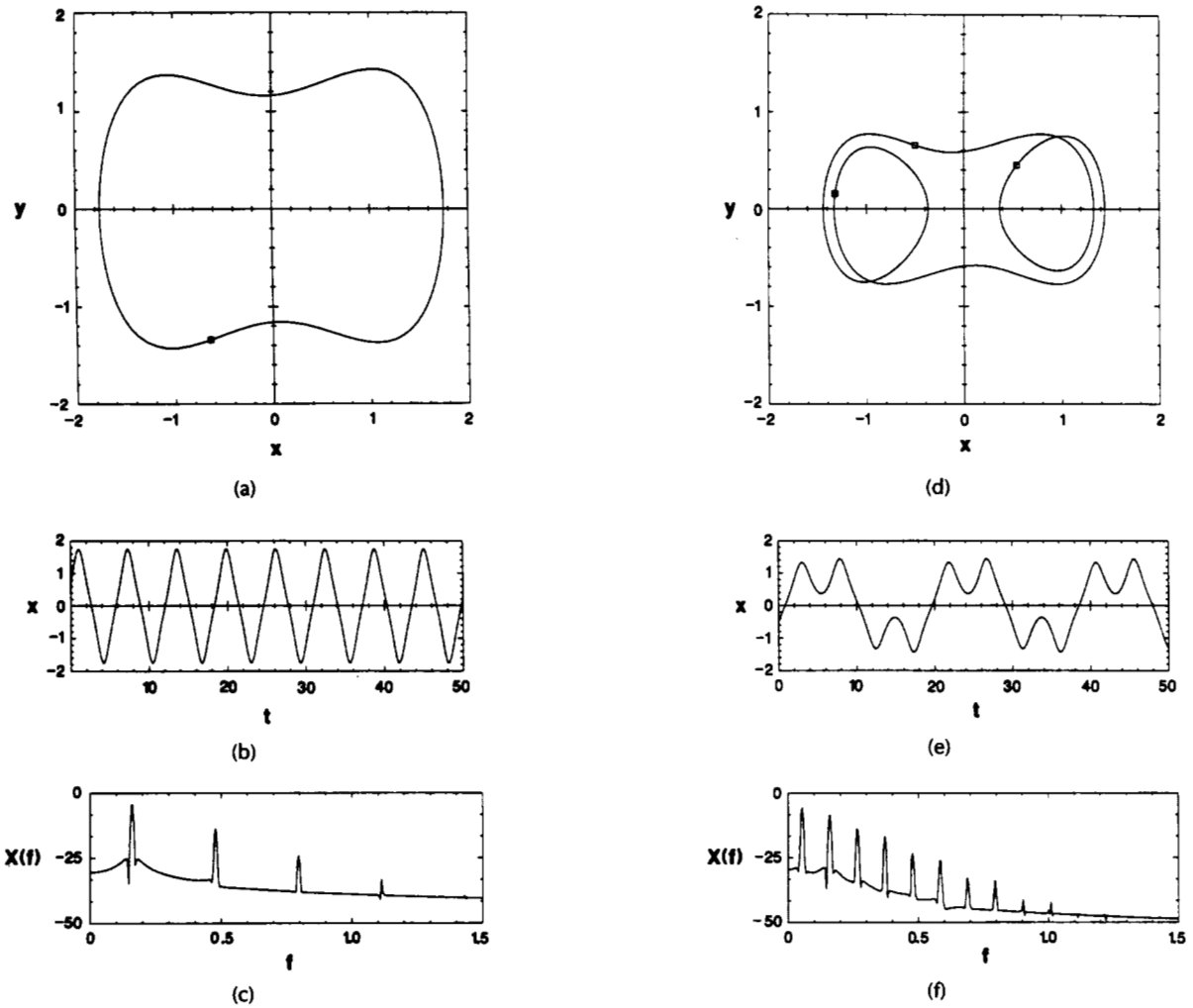

Fig. Fig. 2. Periodic solutions of Duffing's equation for $\gamma = 0.3, \omega = 1$. (a) Period 1 solution $\delta = 0.15$. The square indicates the limit set of the Poincaré map with $t_0 = 0$. (b) Time waveform of first component of (a). (c) Spectrum of first component of (a); due to the symmetry of the time waveform, only odd harmonics are present. (d) Period 3 subharmonic $\delta = 0.22$. The squares indicate the limit set of the Poincaré map with $t_0 = 0$. (e) Time waveform of first component of (d). (f) Spectrum of first component of (d); again only the odd harmonics are present.

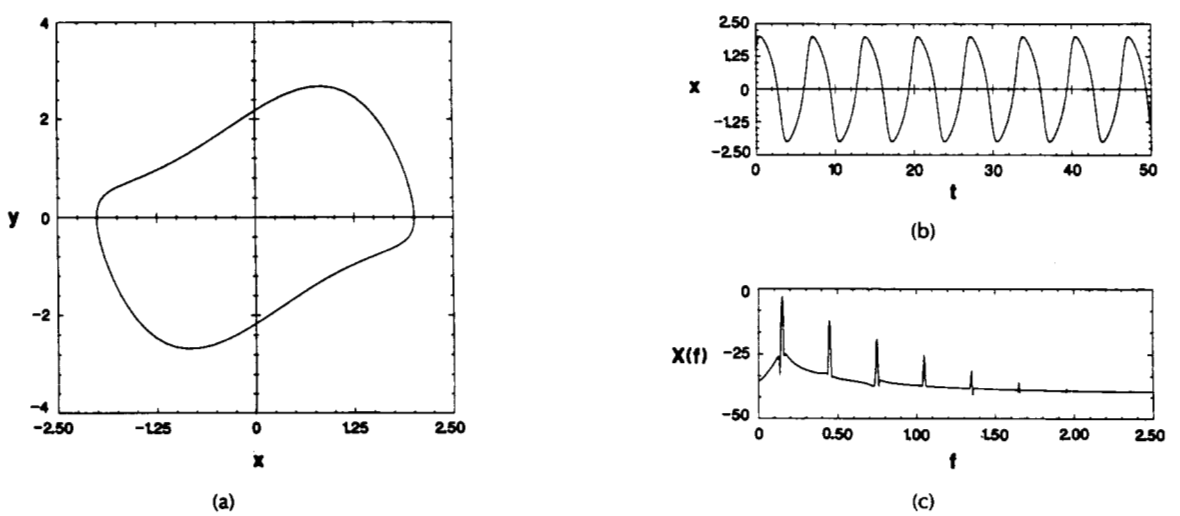

Fig. 3. Limit cycle for the van der Pol equation. (a) Trajectory. (b) Time waveform of first component of (a). (c) Spectrum of first component of (a)—due to the symmetry of the time waveform, only the odd harmonics are present.

The damping term, $(x^2 - 1)$, is negative for $|x| < 1$ implying an expanding solution while it is positive for $|x| > 1$ indicating a contracting solution. Since trajectories near the origin expand, trajectories from the outer regions contract, and the only equilibrium point is 0, there must be a limit cycle encircling the origin; otherwise, the trajectory, constrained to lie on the plane, would intersect itself.

The limit set corresponding to a limit cycle is the closed curve traced out by $\phi_t(x^*)$ over one period. This limit set is a diffeomorphic copy of the circle S, and it is often convenient ot think of limit cycles as circles.

C. Quasi-Periodic Solutions

A *quasi-periodic* solution is one that can be written as a sum of periodic functions

$$x(t) = \sum_i h_i(t) \tag{11}$$

where h_i has minimal period T_i and frequency $f_i = 1/T_i$. Furthermore, there exists a finite set of *base frequencies* $\{\hat{f}_1, \cdots, \hat{f}_p\}$ with the following two properties:

i) It is linearly independent; that is, there does not exist a nonzero set of integers $\{k_1, \cdots, k_p\}$ such that $k_1 \hat{f}_1 + \cdots + k_p \hat{f}_p = 0$.

ii) It forms a finite integral base for the f_i; that is, for each i, $f_i = k_1 \hat{f}_1 + \cdots + k_p \hat{f}_p$ for some integers $\{k_1, \cdots, k_p\}$.

In words, a quasi-periodic waveform is the sum of periodic waveforms each of whose frequency is one of the various sums and differences of a finite set of base frequencies. Note that the base frequencies are not uniquely defined, but that p is. A quasi-periodic solution with p base frequencies is called *p-periodic*.

A periodic waveform is a quasi-periodic waveform with $p = 1$.

The simplest case of a two-periodic function is

$$x(t) = h_1(t) + h_2(t) \tag{12}$$

where T_1 and T_2 are incommensurate.[9] The spectrum of such a waveform consists of two sets of harmonics. The first set, positioned at frequencies k/T_1, $k = 1, 2, \cdots$, corresponds to $h_1(t)$, and the second set, with fundamental frequency $1/T_2$, corresponds to $h_2(t)$.

Here are two examples of two-periodic functions that arise naturally in Electrical Engineering:

1) Amplitude Modulation:

$$x(t) = m(t) \sin (2\pi f_c t) \tag{13}$$

where the message $m(t)$ is periodic. It is well known that the spectrum of $x(t)$ consists of spikes at frequencies $f_c + kf_m$ where f_m is the fundamental frequency of $m(t)$ and k takes on integer values. If f_c and f_m are incommensurate, then $x(t)$ is quasi-periodic with $p = 2$ and base frequencies $\{f_c, f_m\}$.

2) Phase Modulation:

$$x(t) = \sin (2\pi f_c t + m(t)). \tag{14}$$

If $m(t)$ is periodic with fundamental frequency f_m, then the spectrum has spikes at the same locations as the AM spectrum and if f_m and f_c are incommensurate, $x(t)$ is a two-periodic function with frequency base $\{f_c, f_m\}$.

[9]Two real numbers are *incommensurate* if their ratio is irrational.

Neither of these examples has been presented as a solution of a dynamical system, but they do demonstrate one important point: quasi-periodic waveforms may be created when two or more periodic functions interact nonlinearly. In the AM case, the nonlinearity is $g(u, v) = uv$ with $x(t) = g(m(t), \sin (2\pi f_c t))$. For the phase-modulation example, the nonlinearity $g(u, t) = \sin (2\pi f_c t + u)$ is time-periodic and the two-periodic waveform is $x(t) = g(m(t), t)$.

To see how quasi-periodic solutions arise in dynamical systems, consider the van der Pol equation (9). It possesses a limit cycle whose natural period T_1 depends on the system parameters. Now add a sinusoidal forcing term as follows:

$$\begin{aligned} \dot{x} &= y \\ \dot{y} &= (1 - x^2)\, y - x + A \cos (2\pi t/T_2). \end{aligned} \tag{15}$$

The solution to the forced system could synchronize with some multiple of the input period T_2 resulting in a subharmonic. It is also possible that in the conflict between T_1 and T_2, neither period wins, and quasi-periodic behavior is observed.

A two-periodic trajectory of the forced van der Pol equation (15) is shown with a time waveform and its spectrum in Fig. 4. The trajectory is confined to an annular-like region of the state space and is uniformly distributed in this region. Not all two-periodic trajectories exhibit these two char-

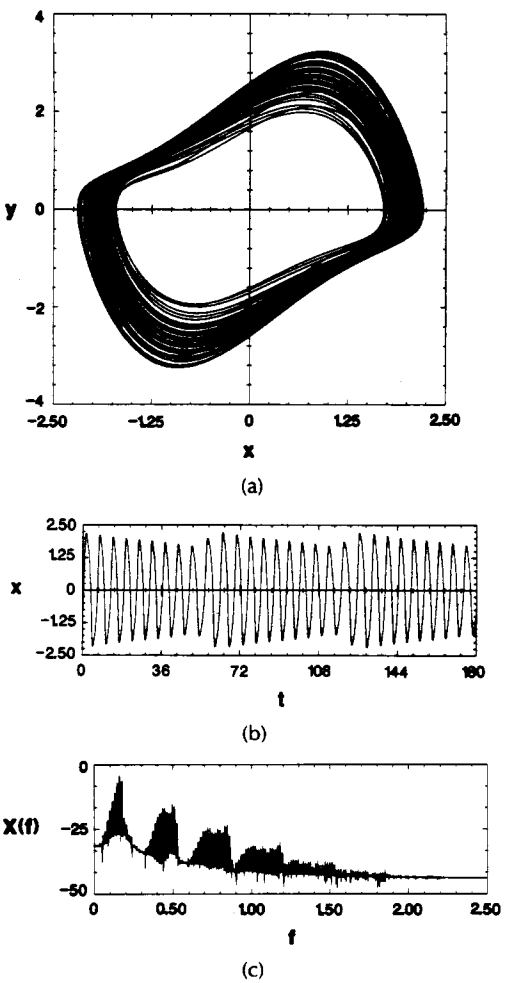

Fig. 4. Quasi-periodic behavior of the non-autonomous van der Pol equation for $A = 0.5$ and $T_2 = 2\pi/1.1$. (a) Trajectory. (b) Time waveform of first component of (a). (c) Spectrum of first component of (a).

acteristics, but their presence is a good indication of two-periodic behavior. The time waveform is clearly amplitude-modulated and since the zero crossings are not uniformly spaced, it is frequency-modulated as well. The spectrum consists of the spectrum of the unforced system (Fig. 3(c)) with tightly spaced sidebands due to the relatively slow modulation. To within measurement error, the spacing of the harmonics within the sidebands is the difference between the natural frequency and the forcing frequency.

It is often difficult to determine whether a solution is quasi-periodic by looking at the spectrum alone. Indeed, without additional confirmation, one could argue that Fig. 4(c) is, in fact, a periodic solution with many of the harmonics missing (including the fundamental). Fortunately, in state space, quasi-periodic trajectories appear quite dif ferent from periodic trajectories, and using both trajectories and spectra, classification is not difficult. In the next section, another method for identifying quasi-periodic solutions will be presented.

A two-periodic trajectory lies on a diffeomorphic copy of the two-torus $S \times S$, each S representing one of the base frequencies (Fig. 5). Since a trajectory is a curve and the two-

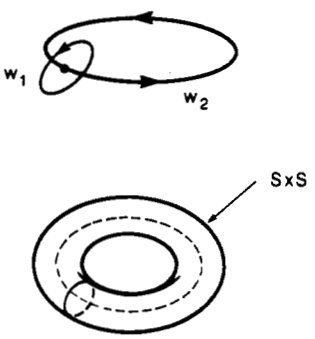

Fig. 5. Two-periodic behavior lies on a two-torus $S \times S$. Each S represents one periodic component.

torus a surface, not every point on the torus lies on the trajectory; however, it can be shown that the trajectory repeatedly passes arbitrarily closely to every point on the torus and, therefore, the torus is the limit set of the quasi-periodic behavior. It is the first example we have seen of a limit set that is not a single trajectory.

Higher order quasi-periodic trajectories can occur in higher order dynamical systems. In general, a quasi-periodic solution with base dimension p possesses a limit set that is diffeomorphic to a p-torus.

D. Chaos

There is no generally accepted definition of chaos. From a practical point of view chaos can be defined as none of the above; that is, as bounded steady-state behavior that is not an equilibrium point, not periodic, and not quasi-periodic. The key question is, "If it is not any of these, then what is it?"

To start the discussion, several examples of chaotic trajectories are shown in Fig. 6. It is evident from these pictures that the trajectories are, indeed, bounded, that they are not periodic, and that they do not have the uniform distribution characteristic of quasi-periodic solutions. Though this last observation does not rule out quasi-periodic behavior, the spectra of the chaotic trajectories do. As shown in Fig. 6, a chaotic spectrum is not composed solely of discrete frequencies, but has a continuous, broad-band nature. This noise-like spectrum is characteristic of chaotic systems.

The limit set for chaotic behavior is not a simple geometrical object like a circle or a torus, but is related to fractals and Cantor sets [6]. This topic will be discussed further when several methods for classifying chaotic limits are presented in Sections V and VI.

Another property of chaotic systems is *sensitive dependence on initial conditions*: given two different initial conditions arbitrarily close to one another, the trajectories emanating from these points diverge at a rate characteristic of the system until, for all practical purposes, they are uncorrelated (Fig. 7). In practice, the initial state of a system can never be specified exactly, but only to within some tolerance $\epsilon > 0$; if two initial conditions x_0 and $\hat{x}_0$ lie within ϵ of one another, they cannot be distinguished. However, after a finite amount of time, $\phi_t(x_0)$ and $\phi_t(\hat{x}_0)$ will diverge and become unrelated. Therefore, no matter how precisely the initial condition is known, the long-term behavior of a chaotic system can never be predicted.[10] This unpredictability is what was meant in the Introduction when chaotic systems were described as "deterministic systems that exhibit random behavior."

Random behavior in a deterministic system may seem surprising at first, but there are many simple examples. For instance, pseudo-random number generators have been used for decades. As another example, consider the one-dimensional discrete-time system

$$x_{k+1} = f(x_k) := 10x_k \bmod 1, \qquad x_0 \in [0, 1]. \tag{16}$$

If x_0 is written as a decimal number

$$x_0 = \sum_{i=1}^{\infty} d_i\, 10^{-i} = 0.d_1 d_2 d_3 \cdots \tag{17}$$

where $d_i \in \{0, \cdots, 9\}$, then the action of f is to drop d_1 and shift the remaining digits one to the left. Thus

$$x_k = \sum_{i=1}^{\infty} d_{k+i}\, 10^{-i} = 0.d_{k+1} d_{k+2} d_{k+3} \cdots . \tag{18}$$

Under repeated applications of f, the most significant digits are lost and less significant digits become more significant until they, too, are discarded one by one.

To show this system is unpredictable, assume the exact initial condition is $x_0 = 1/\sqrt{2} = 0.70710678 \cdots$, but that an observer can measure the state to only three significant figures. The observer can predict that

$$0.7065 < x_1 < 0.7075$$

$$0.065 < x_2 < 0.075$$

$$0.65 < x_3 < 0.75 \tag{19}$$

but can say nothing about x_4 and beyond. For this system, the observed initial condition loses predictive power as time increases. Also note that if the observer measures the state after each iteration (with the same precision as before), the initial conditon can be reconstructed by selecting the first digit of each measurement. In other words, by repeating measurements, the observer gains information about the state as the system evolves.

The rate of loss of predictive power is equal to the rate of information gain and, in fact, these two properties are

[10]Of course, in theory, if the initial condition could be specified to infinite precision, the trajectory could be predicted precisely.

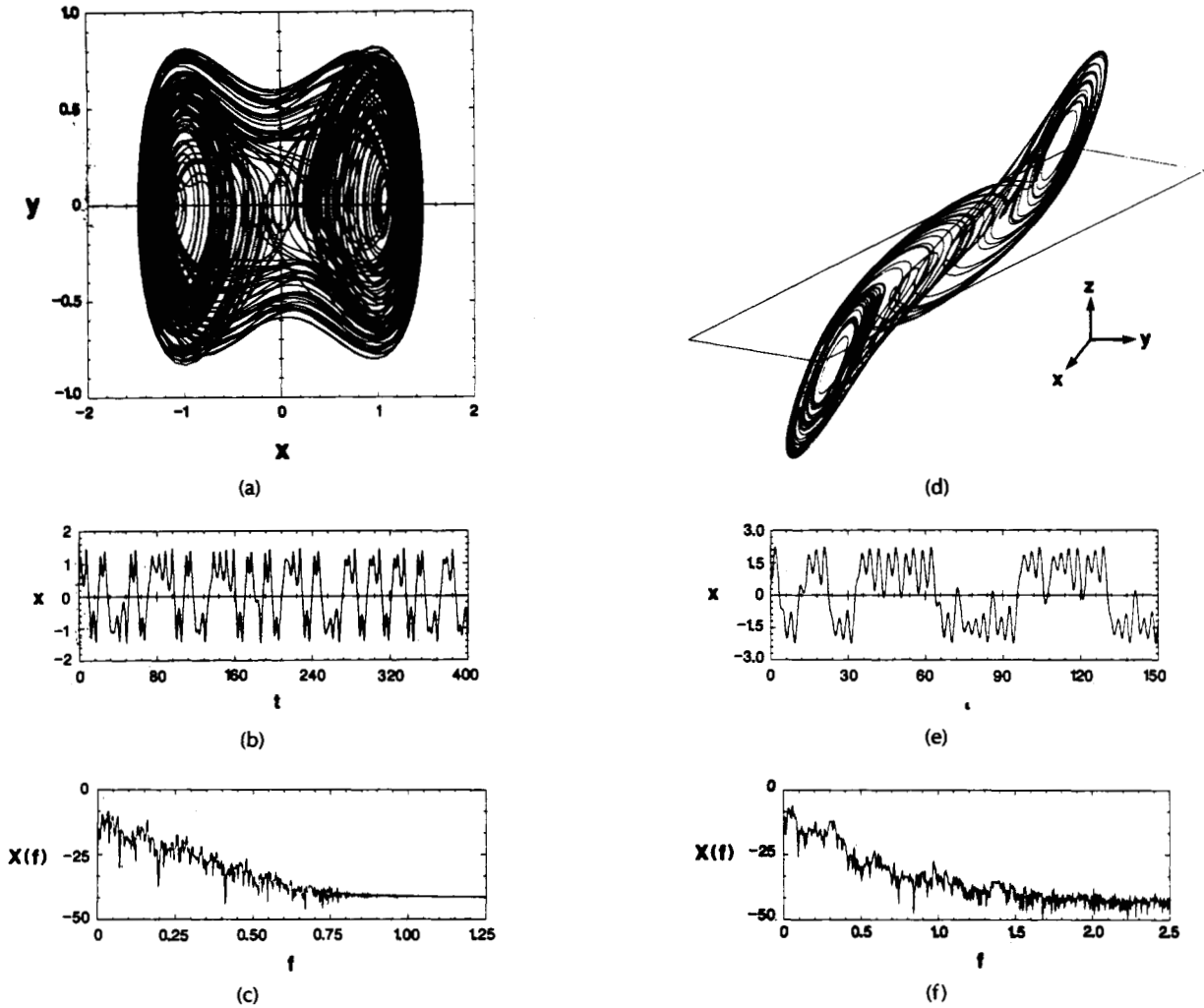

Fig. 6. Chaotic trajectories. (a) Chaotic trajectory of a second-order nonautonomous system (Duffing's equation: $\delta = 0.25$, $\gamma = 0.3$, $\omega = 1.0$). (b) Time waveform of first component of (a). (c) Spectrum, of first component of (a). (d) Chaotic trajectory of a third-order autonomous system (Double Scroll equation). (e) Time waveform of first component of (d). (f) Spectrum of first component of (d).

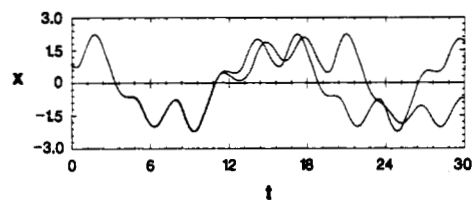

Fig. 7. Two trajectories plotted versus time showing sensitive dependence on initial conditions in a third-order autonomous system (Double Scroll). The initial conditions for the trajectories differ by 0.01 percent.

just different ways of describing the same phenomenon. In this example, the rate is one digit per iteration. The rate is system-dependent; if the 10 in f is replaced by 100, the rate becomes two digits per iteration.

This example is a noninvertible map and it could be argued that it has no direct bearing on continuous-time systems.[11] We now examine how the concepts of information gain and loss of predictive power carry over to the continuous-time case.

E. Information Gain in Continuous-Time Systems

For simplicity, consider an autonomous system with a contracting flow ϕ_t.[12] Suppose that the state of the system can be measured to within a resolution of ϵ; that is, if the state is observed to be x, the actual state lies somewhere in $B_\epsilon(x)$, the ϵ-ball centered at x. Assume there are two observers who measure the state of the system at two different times. Observer 1 observes the state of the system at time t_1 to be x_1. Observer 2 measures the state at time $t_2 > t_1$ to be x_2. Which observer knows more about the state of the system, observer 1 or 2?

Observer 1 knows that the state at t_1 lies somewhere inside $B_\epsilon(x_1)$ and, therefore, that the state at t_2 must lie inside $\phi_{t_2-t_1}(B_\epsilon(x_1))$ (see Fig. 8(a)). Observer 2 knows that the state at t_2 lies somewhere inside $B_\epsilon(x_2)$. However, since ϕ_t is

[11]Remember that the flow of a dynamical system is a diffeomorphism and, therefore, invertible.

[12]ϕ_t is *contracting* if $\|\phi_t(x_0) - \phi_t(\hat{x}_0)\| < \|x_0 - \hat{x}_0\|$ for any $x_0 \neq \hat{x}_0$ and any $t > 0$.

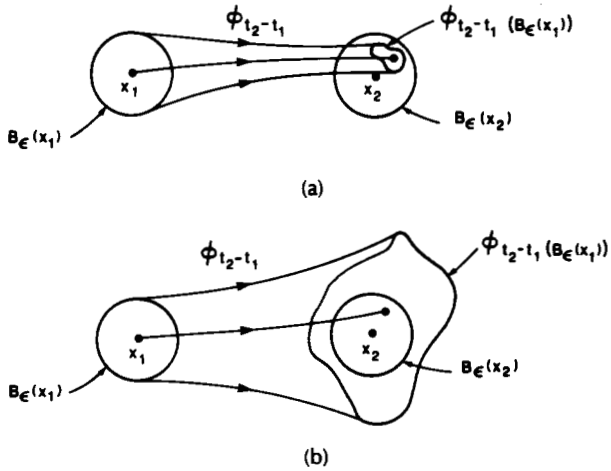

Fig. 8. Information is destroyed in a contracting flow and created in an expanding flow. Observer 1 knows that the state at time t_1 lies inside $B_\epsilon(x_1)$. Observer 2 knows that the state at time $t_2 > t_1$ lies inside $B_\epsilon(x_2)$. (a) If the flow is contracting, $\phi_{t_2-t_1}(B_\epsilon(x_1))$ is smaller than $B_\epsilon(x_2)$ and the earlier observer, observer 1, knows the state of the system more precisely than the latter observer. (b) For an expanding flow, the latter observer, possesses more precise information about the state of the system.

assumed to be contracting, $\phi_{t_2-t_1}(B_\epsilon(x_1))$ is a proper subset of $B_\epsilon(x_2)$ and, therefore, observer 1 knows the state of the system more accurately. Since an earlier observer possesses more information about the state of the system, a contracting system may be thought of as destroying information.

Now consider the opposite case of an expanding flow (Fig. 8(b)). The later observer, number 2, knows more about the state of the system because $B_\epsilon(x_2)$ is contained in $\phi_{t_2-t_1}(B_\epsilon(x_1))$. The longer one waits to observe the state, the more one learns. In other words, an expanding flow may be viewed as creating information.

If the concepts of creating and destroying information are somewhat unintuitive, think of it this way: For a contracting system, it is more accurate to use x_1 to predict the state at time t_2 than to observe the state at t_2. The larger $t_2 - t_1$ is, the greater the accuracy of the prediction. Thus for a contracting (information-destroying) system, the predictive value of the initial condition increases with time. On the other hand, for an expanding (information-creating) system, the predictive value of the initial condition deteriorates with time.

This argument shows that expanding systems exhibit sensitive dependence on initial conditions, but a purely expanding flow also implies unbounded behavior. By definition, a chaotic trajectory is bounded. It follows that a chaotic system must contract in some directions and expand in others with the contraction outweighing the expansion.[13] Lyapunov exponents are used to quantify the expansion and contraction occurring in a dynamical system and are presented in Section V.

An example of an invertible, discrete-time system with both contraction and expansion is the Smale horseshoe which maps the square into itself (Fig. 9(a)) [7]. As is shown

[13]We consider only *dissipative systems* in this tutorial, i.e., systems where volumes in state space contract. For lossless systems, the contraction exactly balances the expansion.

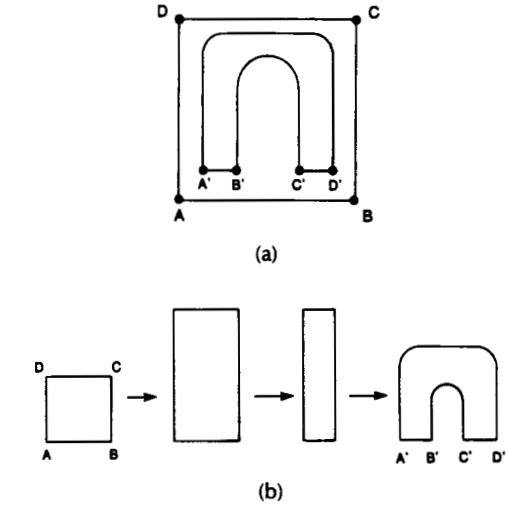

Fig. 9. The Smale horseshoe map. (a) One iteration maps the square *ABCD* to the horseshoe *A'B'C'D'*. (b) Decomposition of the map into an expansion, a contraction and a folding.

in Fig. 9(b), one iteration of the horseshoe map is composed of three simple operations: stretching gives the expansion; squeezing, the contraction; and folding guarantees boundedness. This stretching, squeezing, and folding behavior is typical of chaotic systems.

Now that the different types of steady-state behavior have been defined, the remainder of Part I is dedicated to the presentation of different methods of identifying and classifying this behavior.

IV. The Poincaré Map

A classical technique for analyzing dynamical systems is due to Poincaré. It replaces the flow of a continuous-time dynamical system with a map called the Poincaré map.

A. The Definition of the Poincaré Map

The definitions of the Poincaré map are slightly different for autonomous and nonautonomous systems, and the two cases are presented separately.

1) The Poincaré Map for Nonautonomous Systems: As was shown in Section II-B, the nth-order nonautonomous system (2) with period T may be transformed into an $(n + 1)$-dimensional autonomous system (3) in cylindrical state space $\mathbb{R}^n \times S$.

Consider the n-dimensional hyper-plane Σ in $\mathbb{R}^n \times S$ defined by

$$\Sigma = \{(x, \theta) \in \mathbb{R}^n \times S | \theta = \theta_0\}. \tag{20}$$

Every T seconds, the trajectory (4) intersects Σ (Fig. 10). Thus a map P: $\Sigma \to \Sigma$ ($:\mathbb{R}^n \to \mathbb{R}^n$) is defined by $P(x) = \phi_T(x, t_0)$. P is called the *Poincaré map*. Note that ϕ_T is a diffeomorphism and, therefore, P is one-to-one and differentiable.

P may be thought of in two ways.

i) $P(x)$ indicates where the flow takes x after T seconds. This is called a T-advance mapping.
ii) The orbit $\{P^k(x)\}_{k=-\infty}^{\infty}$ is a sampling of a single trajectory every T seconds; that is,

$$P^k(x_0) = \phi_{kT}(x_0, t_0), \qquad \text{for } k = 0, 1, \cdots.$$

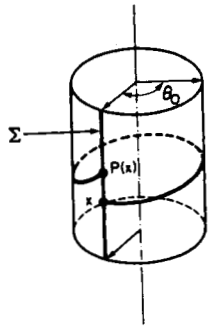

Fig. 10. The Poincaré map of a first-order nonautonomous system. When transformed to an autonomous system, the state space is the cylinder $R \times S$. The cross section Σ is the line defined by $\theta = \theta_0$. $P(x)$ is the first point where the trajectory emanating from x intersects Σ.

This is similar to the action of a stroboscope flashing with period T.

2) The Poincaré Map for Autonomous Systems: Consider an nth-order autonomous system with the limit cycle Γ shown in Fig. 11. Let x^* be a point on the limit cycle and let

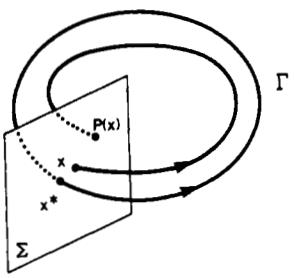

Fig. 11. The Poincaré map for autonomous system is defined by a limit cycle Γ and a cross section Σ.

T be the minimal period of the limit cycle. Take an $(n-1)$-dimensional hyper-plane Σ transverse[14] to Γ at x^*. The trajectory emanating from x^* will hit Σ at x^* in T seconds. Due to the continuity of ϕ_t with respect to the initial condition, trajectories starting on Σ in a sufficiently small neighborhood of x^* will, in approximately T seconds, intersect Σ in the vicinity of x^*. Hence, f and Σ define a mapping P of some neighborhood $U \subset \Sigma$ of x^* onto another neighborhood $V \subset \Sigma$ of x^*. P is called the *Poincaré map* or *first-return map*.

It is important to realize that for autonomous systems, the Poincaré map is defined only in a neighborhood of x^*; unlike the nonautonomous case, it is not guaranteed that the trajectory emanating from any point on Σ will intersect Σ again. As in the nonautonomous case, it can be shown that P is a diffeomorphism [3].

The definition just presented is the standard one from the theory of dynamical systems, but it is often impractical in experimental settings because it requires advance knowledge of the position of a limit cycle. In practice, one chooses an $(n-1)$-dimensional hyper-plane

$$\Sigma := \{x: h^T(x - x_\Sigma) = 0\} \tag{21}$$

[14]In this setting, *transverse* means *not tangent.*

where h is a vector normal to Σ and x_Σ is some point lying on the hyper-plane. Σ divides the state space into two regions

$$\Sigma^+ := \{x: h^T(x - x_\Sigma) > 0\} \tag{22a}$$

and

$$\Sigma^- := \{x: h^T(x - x_\Sigma) < 0\}. \tag{22b}$$

If Σ is chosen properly, the trajectory under observation repeatedly passes through Σ, crossing from Σ^- to Σ^+ to Σ^-, etc. The sequence of Σ^- to Σ^+ crossings defines a map in the obvious way as do the Σ^+ to Σ^- crossings (Fig. 12). These

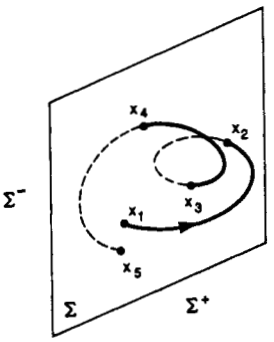

Fig. 12. A typical trajectory intersecting a cross section Σ. The points $\{x_1, x_3, x_5, \cdots\}$ are an orbit of the one-sided Poincaré map defined by crossings that pass from Σ^- and Σ^+. The entire sequence of points $\{x_1, x_2, x_3, \cdots\}$ is an orbit of the double-sided Poincaré map.

maps are called *one-sided* Poincaré maps since the only crossings that matter are those from one side of Σ. The entire sequence of crossing points taken without regard for crossing direction defines a *two-sided* Poincaré map.

B. Steady-State Behavior of the Poincaré Map

The usefulness of the Poincaré map stems from the fact that there is a one-to-one correspondence between the different types of steady-state behavior of the underlying continuous-time dynamical system and the steady-state behavior of P.

1) Poincaré Maps and Periodic Solutions: As is clear from the definition of P, a period-one solution of the underlying flow corresponds to a fixed point of the Poincaré map; that is, $P(x) = x$ implies that x lies on a periodic solution. The small square in Fig. 2(a) indicates the position of the fixed point for that period-one trajectory with $t_0 = 0$.

For nonautonomous systems, a closed orbit of P with period K, corresponds to a Kth-order subharmonic of the flow. The three small squares in Fig. 2(d) indicate the closed orbit of the Poincaré map corresponding to the third-order subharmonic again with $t_0 = 0$. In the autonomous case, there are some circumstances (e.g., a period-doubling bifurcation) where a closed orbit of P may be thought of as a subharmonic of the autonomous system. One must be careful with this interpretation, however, since, unlike a nonautonomous system, there is no unique period in terms of which a subharmonic can be defined.

2) Poincaré Maps and Quasi-Periodicity: The Poincaré map is useful for detecting quasi-periodic as well as periodic behavior. We have seen earlier that two-periodic solutions lie on a diffeomorphic copy of the two-torus $S \times S$.

Using coordinates (θ_1, θ_2) on the torus, a two-periodic trajectory may be written

$$\begin{bmatrix} \theta_1(t) \\ \theta_2(t) \end{bmatrix} = \begin{bmatrix} 2\pi f_1 t \bmod 2\pi \\ 2\pi f_2 t \bmod 2\pi \end{bmatrix} \tag{23}$$

where f_1 and f_2 are incommensurate frequencies.

In the nonautonomous case, one of the frequencies, f_1, say, is the forcing frequency of the system. An orbit of the Poincaré map corresponds to sampling (23) every $1/f_1$ seconds

$$\begin{bmatrix} \theta_1(k/f_1) \\ \theta_2(k/f_1) \end{bmatrix} = \begin{bmatrix} 2\pi k \bmod 2\pi \\ 2\pi k f_2/f_1 \bmod 2\pi \end{bmatrix} \tag{24a}$$

$$= \begin{bmatrix} 0 \\ 2\pi k f_2/f_1 \bmod 2\pi \end{bmatrix}, \quad k = 0, 1, \cdots. \tag{24b}$$

Hence, the Poincaré map acts like a stroboscope; it freezes any component of the behavior that occurs at the sampling frequency. Since f_1 and f_2 are incommensurate, $\{\theta_2(k/f_1)\}_{k=0}^{\infty}$ is not periodic and repeatedly comes arbitrarily close to every point in $[0, 2\pi)$. Thus in the (θ_1, θ_2) coordinate system, the limit set of the Poincaré map is the circle S. In the original Euclidean coordinates, the limit set is a diffeomorphic copy of the circle. The Poincaré limit set for the nonautonomous van der Pol system (15) is shown in Fig. 13.

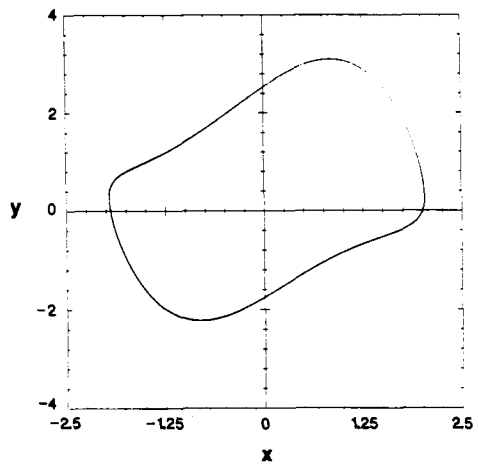

Fig. 13. An orbit of the Poincaré map in the nonautonomous two-periodic case. The limit set of the Poincaré map is a diffeomorphic copy of a circle.

In the two-periodic autonomous case, the geometry of the Poincaré limit set depends on the orientation of the cross section Σ with respect to the two-torus and whether a single- or double-sided map is used. If Σ passes through the hole of the torus, the limit set of the single-sided map is (a diffeomorphic copy of) a circle and if a two-sided Poincaré map is used, two circles are obtained (Fig. 14(a)). If Σ does not pass through the hole of the torus, the limit set of the single-sided map is an arc of a circle, and the double-sided limit set is the entire circle (Fig. 14(b)).

To summarize, in both autonomous and nonautonomous systems, the limit set of the Poincaré map for two-periodic behavior is a diffeomorphic copy of a circle (assuming the proper choice of single-sided or double-sided maps for autonomous systems).

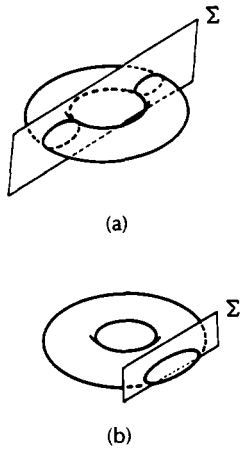

Fig. 14. Limit sets of the Poincaré map in the autonomous two-periodic case. (a) For a typical cross section Σ, the limit set of the two-sided Poincaré map is two closed curves. (b) For a different cross section, the two-sided limit set is a single closed curve.

3) Poincaré Maps and Chaos: The steady-state Poincaré orbits of chaotic systems are distinctive and often quite beautiful. A few typical orbits are shown in Fig. 15. Looking at these orbits, two points are immediately clear.

First, the steady-state orbits do not lie on a simple geometrical object as is the case with periodic and quasi-periodic behavior. Second, the attractor has a fine structure. As the magnifications in Fig. 15(b), (c) show, there appear to be layers within layers, much like Baklava or a fine French pastry. This fine structure is typical of chaotic systems and will be discussed further in Section VI when the concept of dimension is presented.

V. Stability of Limit Sets

Attracting limit sets are of supreme importance in experimental and numerical settings because they are the only type of limit sets that can be observed. In this section, we examine conditions for a limit set to be attracting.

We start with the familiar case of the eigenvalues at an equilibrium point, move on to the characteristic multipliers of a periodic solution, and finish with Lyapunov exponents.

A. Equilibrium Points

Consider an equilibrium point x_{eq} of (1). It is well known that the local behavior of the flow near x_{eq} is determined by linearizing f at x_{eq}. In particular, the linear vector field

$$\dot{\delta x} = Df(x_{eq})\delta x \tag{25}$$

governs the time evolution of perturbations near the equilibrium point.

The trajectory with initial condition $x_{eq} + \delta x_0$ is, to the first order,

$$\phi_t(x_{eq} + \delta x_0) = x_{eq} + \delta x(t) \tag{26a}$$

$$= x_{eq} + e^{Df(x_{eq})t}\delta x_0 \tag{26b}$$

$$= x_{eq} + c_1\eta_1 e^{\lambda_1 t} + \cdots + c_n\eta_n e^{\lambda_n t} \tag{26c}$$

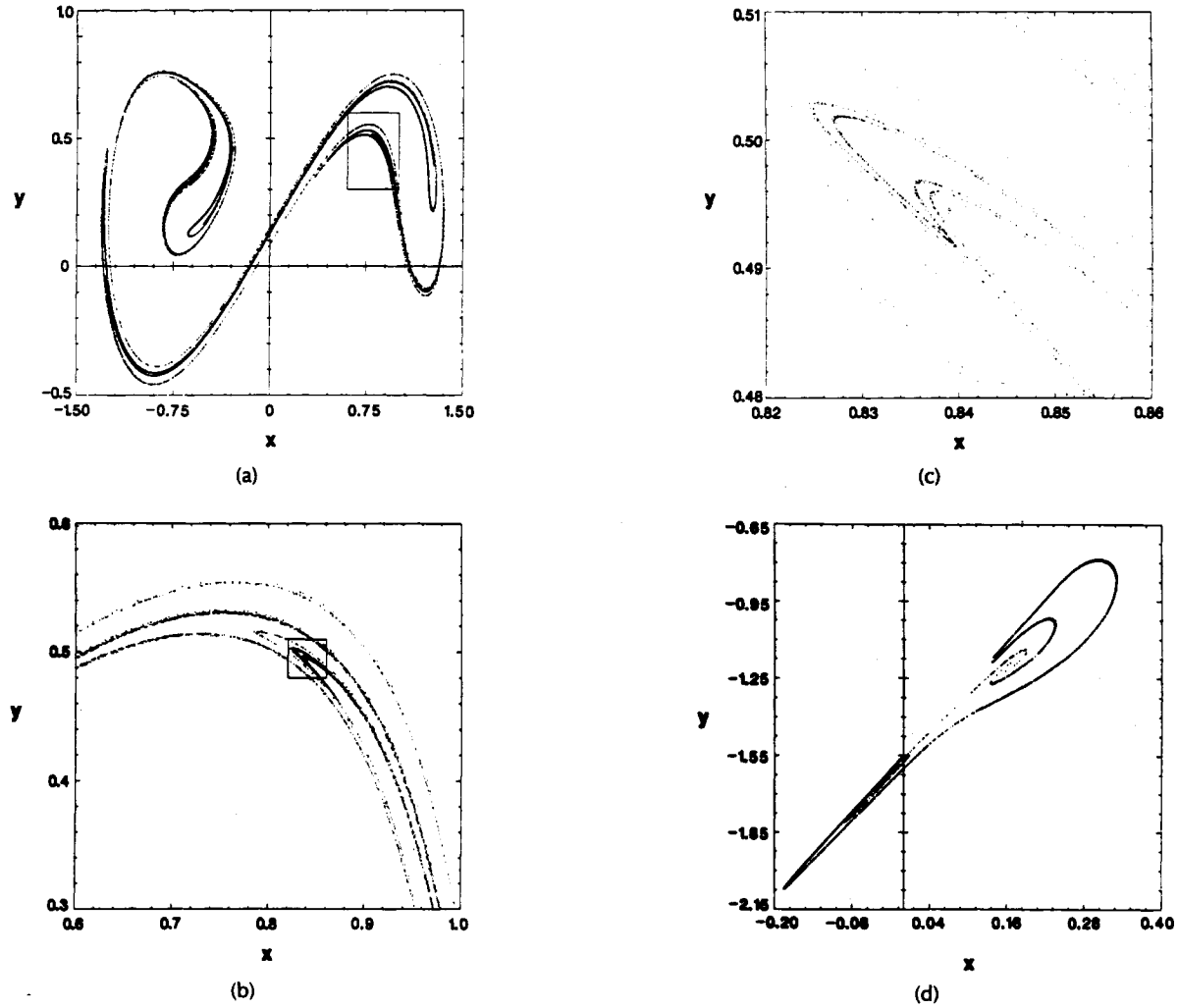

Fig. 15. Chaotic orbits of the Poincaré map corresponding to the trajectories of Fig. 6. (a) Second-order nonautonomous system (Duffing's equation). (b) and (c) are successive magnifications of (a) showing the fine structure of the attractor. (d) Third-order autonomous system (Double Scroll equation).

where $\{\lambda_i\}_{i=1}^n$ and $\{\eta_i\}_{i=1}^n$ are the eigenvalues and eigenvectors of $Df(x_{eq})$ and $\{c_i\}_{i=1}^n$ are scalar constants chosen to achieve the correct initial condition.[15] The real part of λ_i gives the rate of expansion (if Re $[\lambda_i] > 0$) or contraction (if Re $[\lambda_i] < 0$) in the neighborhood of the equilibrium point along the direction of η_i.

If Re $[\lambda_i] < 0$ for all λ_i, then all sufficiently small perturbations tend toward 0 as $t \to \infty$ and x_{eq} is *asymptotically stable*. If some Re $[\lambda_i] > 0$, then x_{eq} is not stable and is either *unstable* (all Re $[\lambda_i] > 0$) or *nonstable* (some Re $[\lambda_i] < 0$ and some Re $[\lambda_i] > 0$). The unstable/nonstable distinction is helpful because an unstable equilibrium point becomes stable in reverse time and a nonstable equilibrium point remains nonstable when the flow is reversed. A nonstable equilibrium point is often called a *saddle point*.

If one of the eigenvalues has zero real part, then the stability cannot be determined from the eigenvalues alone. Equilibrium points where all the eigenvalues have nonzero real part are termed *hyperbolic*. Hyperbolic equilibrium points have the useful property of structural stability, that is, they still exist under small perturbations of the vector field and the perturbed equilibrium point has the same stability type. Typically, nonhyperbolic equilibrium points are not structurally stable and therefore cannot be observed experimentally or in simulations.

[15] In (26c) it is assumed that the λ_i are distinct; however, the following results on stability are valid in general.

B. Periodic Solutions

The stability of a periodic solution is determined by its *characteristic multipliers*, also called *Floquet multipliers*. Characteristic multipliers are a generalization of the eigenvalues at an equilibrium point.

A periodic solution corresponds to a fixed point of the Poincaré map P. Not surprisingly, the stability of the periodic solution is determined by the stability of the fixed point. By analogy with an equilibrium point, the stability of a fixed point x^* of P is determined by linearizing P at x^*. The linear discrete-time system

$$\delta x_{k+1} = DP(x^*)\delta x_k \tag{27}$$

governs the local behavior of P near x^*.

Let p be the dimension of $DP(x^*)$; p equals n for nonautonomous systems and $(n-1)$ for autonomous systems. The orbit of P for an initial condition $x_0 + \delta x_0$ is, to first order,[16]

$$x_k = x^* + \delta x_k \tag{28a}$$

$$= x^* + DP(x^*)^k \delta x_0 \tag{28b}$$

$$= x^* + c_1\eta_1 m_1^k + \cdots + c_p\eta_p m_p^k \tag{28c}$$

where $\{m_i\}_{i=1}^p$ and $\{\eta_i\}_{i=1}^p$ are the eigenvalues and eigenvectors of $DP(x^*)$, and $\{c_i\}_{i=1}^p$ are scalar constants chosen to achieve the correct initial condition.[17]

The eigenvalues $\{m_i\}$ are the characteristic multipliers of the fixed point and determine the amount of contraction ($|m_i| < 1$) and expansion ($|m_i| > 1$) near x^* in the direction of η_i for one iteration of the map P.

It is shown in [1] that as long as Σ is transverse to the periodic solution, the characteristic multipliers are independent of the orientation and position of the cross section Σ, and it makes sense to speak of *the* characteristic multipliers of a periodic solution.

The characteristic multipliers determine the stability of the periodic solution. If all of the m_i lie within the unit circle, then the periodic solution is asymptotically stable. If all $|m_i| > 1$, the periodic solution is unstable. If some characteristic multipliers lie within the unit circle and others lie outside it, then the periodic solution is nonstable.

If one of the characteristic multipliers lies on the unit circle, then the stability of the periodic solution cannot be determined by the multipliers alone. By analogy with equilibrium points, periodic solutions with no characteristic multipliers on the unit circle are termed hyperbolic. Hyperbolic periodic solutions are structurally stable.

We have established that the eigenvalues of $DP(x^*)$ are of special interest, but how can $DP(x^*)$ be calculated? We start with the easier case of nonautonomous systems.

1) Characteristic Multipliers of Nonautonomous Systems: In the nonautonomous case, $P(x) := \phi_T(x, t_0)$ so

$$DP(x^*) = D_{x_0}\phi_T(x^*, t_0) =: \Phi_T(x^*, t_0) \tag{29}$$

where $\Phi_T(x^*, t_0)$ denotes the derivative[18] of $\phi_T(x^*, t_0)$ with respect to the initial condition.

$\Phi_T(x_0, t_0)$ is the solution to the *variational equation* which can be formally defined by differentiating (2) with respect to the initial condition. First, substitute $\phi_t(x_0, t_0)$ for x in (2)

$$\dot{\phi}_t(x_0, t_0) = f(\phi_t(x_0, t_0), t) \qquad \phi_{t_0}(x_0, t_0) = x_0 \tag{30}$$

and then differentiate with respect to x_0

$$D_{x_0}\dot{\phi}_t(x_0, t_0) = D_x f(\phi_t(x_0, t_0), t)\, D_{x_0}\phi_t(x_0, t_0)$$

$$D_{x_0}\phi_{t_0}(x_0, t_0) = I. \tag{31a}$$

Using the Φ notation defined in (29), rewrite (31a) as

$$\dot{\Phi}_t(x_0, t_0) = D_x f(\phi_t(x_0, t_0))\, \Phi_t(x_0, t_0) \qquad \Phi_{t_0}(x_0, t_0) = I \tag{31b}$$

which can be abbreviated as

$$\dot{\Phi} = D_x f(\phi_t(x_0, t_0), t)\, \Phi \qquad \Phi_0 = I. \tag{31c}$$

Equations (31) are all different forms of the variational equation.

Remarks:

i) $D_x f(\phi_t(x_0, t_0), t)$ is a time-varying matrix and, therefore, the variational equation is a linear time-varying system of order n^2.

ii) $\Phi_t(x_0, t_0)$ is the state transition matrix of the system

$$\dot{\delta x} = D_x f(\phi_t(x_0, t_0), t)\, \delta x \qquad \delta x(t_0) = \delta x_0 \tag{32}$$

that is, $\delta x(t) = \Phi_t(x_0, t_0)\delta x_0$. Here δx can be thought of as a small perturbation of the initial condition of the original system (2). Thus $\Phi_t(x_0, t_0)$ governs the time evolution of small perturbations. To first order

$$\phi_t(x_0 + \delta x_0, t_0) = \phi_t(x_0, t_0) + \Phi_t(x_0, t_0)\delta x_0 \tag{33}$$

for t fixed and δx_0 sufficiently small. This interpretation makes sense since Φ is defined as the derivative of $\phi_t(x_0, t_0)$ with respect to the initial condition.

iii) The variational equation is the linearization of the vector field along a specific trajectory $\phi_t(x_0, t_0)$. If the trajectory is altered by changing x_0 or t_0, then the variational equation changes as well.

2) Characteristic Multipliers of Autonomous Systems: Finding an expression for $DP(x^*)$ is usually impossible for autonomous systems because there is no explicit expression for P. However, we are not interested in $DP(x^*)$; we want its $(n-1)$ eigenvalues. As before, the eigenvalues can be found using the variational equation.

For the autonomous case, the variational equation is

$$\dot{\Phi} = Df(\phi_t(x_0))\Phi \qquad \Phi_0 = I \tag{34}$$

with solution $\Phi_t(x_0)$. It is shown in [1] that the n eigenvalues of $\Phi_T(x^*)$ consist of the $(n-1)$ characteristic multipliers together with an eigenvalue that is always 1.

That one eigenvalue of $\Phi_T(x^*)$ is always equal to 1 for x^* on a limit cycle may be shown by finding some perturbation Δx_0 such that $\Delta x_0 = \Phi_T(x^*)\Delta x_0$. Choose the perturbation tangent to $\phi_t(x^*)$, that is, $\Delta x_0 = \epsilon f(x^*)$ for some small ϵ. Then, to first order, $x^* + \Delta x_0$ lies on the limit cycle (in fact, $x^* + \Delta x_0 \approx \phi_\epsilon(x^*)$) and, therefore, after T seconds, the perturbed trajectory will return to $x^* + \Delta x_0$. Hence, the perturbation Δx_0 maps to Δx_0 in T seconds implying that $\Delta x_0 = \Phi_T(x^*)\Delta x_0$ as desired.

3) Discussion of Characteristic Multipliers: To summarize, the characteristic multipliers give the amount of contraction or expansion per period near a periodic solution. The n characteristic multipliers of a periodic solution of a nonautonomous system are the eigenvalues of $\Phi_T(x^*, t_0)$. In the autonomous case, at least one eigenvalue of $\Phi_T(x^*)$ is always equal to 1; the remaining $(n-1)$ eigenvalues are the characteristic multipliers of the limit cycle.

Closed orbits $\{x_k^*\}_{k=1}^K$ of the Poincaré map with period K correspond to Kth-order subharmonics of the underlying dynamical system. Since x_1^* is a fixed point of the K-fold iterated Poincaré map P^K, the stability of the subharmonic is determined by the eigenvalues of $DP^K(x_1^*)$ which can be found from $\Phi_{KT}(x_1^*, t_0)$ in the nonautonomous case or $\Phi_{KT}(x_1^*)$ in the autonomous case. It is arbitrary which of the K points of the closed orbit is called x_1^*, and one can use

[16]Readers familiar with discrete-time systems will recognize these equations as the discrete-time versions of (26). We will show shortly that near an equilibrium point, $m_i = e^{\lambda_i t}$.

[17]In (28c) it is assumed that the m_i are distinct; however, the following results on stability are valid in general.

[18]The notation D_{x_0} means the partial derivative with respect to x_0, i.e., $D_{x_0}\phi_T(x^*, t_0)$ is the Jacobian matrix of the n-vector $\phi_T(x_0, t_0)$ with respect to the n-vector x_0 evaluated at $x_0 = x^*$.

any of the $\Phi_{KT}(x_k^*, t_0)$, $k = 1, \cdots, K$ to calculate the characteristic multipliers.

We now present an example designed to illustrate that characteristic multipliers are a generalization of the eigenvalues at an equilibrium point. Let x_{eq} be an equilibrium point of an autonomous system. Choose $T > 0$. x_{eq} can be treated as a limit cycle with (nonminimal) period T. To find the characteristic multipliers of this "limit cycle," we need to calculate $\Phi_T(x_{eq})$. $\phi_t(x_{eq}) = x_{eq}$ so the variational equation is

$$\dot{\Phi} = Df(x_{eq})\Phi \qquad \Phi_0 = I. \tag{35}$$

This is a linear time-invariant differential equation with state transition matrix $\Phi_t(x_{eq}) = e^{Df(x_{eq})t}$. Let the eigenvalues of $Df(x_{eq})$ be $\{\lambda_i\}_{i=1}^n$. By the spectral mapping theorem [8], the λ_i and the characteristic multipliers m_i are related by $m_i = e^{\lambda_i T}$. Since $|m_i| < 1$ if and only if $\mathrm{Re}\,[\lambda_i] < 0$ and $|m_i| > 1$ if and only if $\mathrm{Re}\,[\lambda_i] > 0$, λ_i and m_i provide the same stability information.[19]

C. Lyapunov Exponents

Lyapunov exponents are a generalization of the eigenvalues at an equilibrium point and of characteristic multipliers. They are used to determine the stability of any type of steady-state behavior including quasi-periodic and chaotic solutions.

Lyapunov exponents are defined in terms of the solution of the variational equation as follows. Let $\{m_i(t)\}_{i=1}^n$ be the eigenvalues of $\Phi_t(x_0)$. The Lyapunov exponents are defined by

$$\lambda_i := \lim_{t\to\infty} \frac{1}{t} \ln |m_i(t)|, \qquad i = 1, \cdots, n \tag{36}$$

if the limit exists.[20]

To gain some familiarity with Lyapunov exponents, we now find the Lyapunov exponents of an equilibrium point x_{eq}. Let $\{\hat{\lambda}_i\}_{i=1}^n$ and $\{\eta_i\}_{i=1}^n$ be the eigenvalues[21] and eigenvectors of $Df(x_{eq})$. As was shown in the previous section, $\Phi_t(x_{eq}) = e^{Df(x_{eq})t}$. It follows that $m_i(t) = e^{\hat{\lambda}_i t}$ and

$$\lambda_i = \lim_{t\to\infty} \frac{1}{t} \ln |e^{\hat{\lambda}_i t}|$$

$$= \lim_{t\to\infty} \frac{1}{t} \mathrm{Re}\,[\hat{\lambda}_i]t = \mathrm{Re}\,[\hat{\lambda}_i]. \tag{37}$$

Hence, in this special case, the Lyapunov exponents are equal to the real parts of the eigenvalues at the equilibrium point and indicate the rate of contraction ($\lambda_i < 0$) or expansion ($\lambda_i > 0$) near the equilibrium point.

Suppose that $x_0 \neq x_{eq}$, but $\phi_t(x_0) \to x_{eq}$ as $t \to \infty$, that is, x_0 is in the basin of attraction of x_{eq}. Since the Lyapunov exponents are defined in the limit as $t \to \infty$, any finite transient may be neglected and, therefore, the Lyapunov exponents of x_0 and x_{eq} are identical. In general, every point in the basin of attraction of an attractor has the same Lyapunov exponents as the attractor.[22]

Likewise, it can be shown that the Lyapunov exponents λ_i of a limit cycle have a simple relationship to the $(n-1)$ characteristic multipliers:

$$\lambda_i = \frac{1}{T} \ln |m_i|, \qquad \text{for } i = 1, \cdots, n-1.$$

One Lyapunov exponent λ_n is always 0. It corresponds to the eigenvalue of $\Phi_T(x^*)$ that is always 1.

As the examples of equilibrium point and limit cycle demonstrate, λ_i is the average rate of contraction ($\lambda_i < 0$) or expansion ($\lambda_i > 0$) in a particular direction near a particular trajectory. What is meant by "in a particular direction?" Order the λ_i such that $\lambda_1 \geq \cdots \geq \lambda_n$. Using this ordering, there are n linear subspaces, $W_1 \supset \cdots \supset W_n$, with dim $W_1 = n$, dim $W_2 = n-1$, $\cdots$, dim $W_n = 1$, such that almost all perturbations in W_i evolve (on the average) as $e^{\lambda_i t}$.

As an example, consider a third-order linear system with an equilibrium point at the origin, real eigenvalues $\lambda_1 > \lambda_2 > \lambda_3$, and corresponding eigenvectors η_1, η_2, η_3. Since the eigenvalues are real, they are equal to the Lyapunov exponents. $W_3 = \mathrm{span}\,\{\eta_3\}$ and all initial conditions $x_0 \in W_3$ evolve as $x_0 e^{\lambda_3 t}$. $W_2 = \mathrm{span}\,\{\eta_2, \eta_3\}$ and all initial conditions $x_0 \in W_2 \backslash W_3$ evolve as $c_2\eta_2 e^{\lambda_2 t} + c_3\eta_3 e^{\lambda_3 t}$. Since $\lambda_2 > \lambda_3$, the λ_3 term becomes negligible after a finite time and, as $t \to \infty$, the trajectory evolves as[23] $e^{\lambda_2 t}$. $W_1 = \mathrm{span}\,\{\eta_1, \eta_2, \eta_3\} = \mathbb{R}^3$ and any $x_0 \in W_1 \backslash W_2$ eventually evolves as $e^{\lambda_1 t}$. Of course, in the nonlinear case, one must speak of an infinitesimal perturbation evolving on the average as $e^{\lambda_i t}$ or, equivalently, of a solution of the linearized system (32) evolving on the average as $e^{\lambda_i t}$.

The proof that one characteristic multiplier of a limit cycle always equals 1 can be generalized to show that for any bounded attractor of an autonomous system except an equilibrium point, one Lyapunov exponent is always 0 [10].

Lyapunov exponents are convenient for categorizing steady-state behavior. For an attractor, contraction must outweigh expansion so

$$\sum_{i=0}^{n} \lambda_i < 0.$$

Attractors are classified as follows.[24] For stable equilibrium points, $\lambda_i < 0$ for all i. For a stable limit cycle, $\lambda_1 = 0$ and $\lambda_i < 0$ for $i = 2, \cdots, n$. For a stable torus, $\lambda_1 = \lambda_2 = 0$ and $\lambda_i < 0$ for $i = 3, \cdots, n$.

One feature of chaos is sensitive dependence on initial conditions. As was explained in Section III, sensitive dependence occurs in an expanding flow. Hence, what distinguishes a strange attractor from the other types of attractor is the existence of at least one positive Lyapunov exponent. In the three-dimensional case, keeping in mind that $\Sigma\lambda_i <$

[19]An equilibrium point has zero minimal period and is not a true limit cycle. The difference is apparent in this example since none of the eigenvalues of $\Phi_T(x_{eq})$ is equal to 1 as is required for a true limit cycle.

[20]*lim* can be replaced by *lim sup* to guarantee existence of the Lyapunov exponents; however, the interpretation of Lyapunov exponents presented shortly is only correct when the limit in (36) exists.

[21]It is common to use λ for both eigenvalues and Lyapunov exponents. In this section, we use $\hat{\lambda}$ for eigenvalues in order to distinguish the two.

[22]This statement may need to be changed to *almost every point* for some definitions of strange attractor, but is always true for nonstrange attractors.

[23]A geometrical interpretation of this behavior is given in [9].

[24]This classification scheme is generic in that it ignores nonhyperbolic attractors.

Table 1 Classification of Attracting Sets

Steady State	Attracting Set: Flow	Attracting Set: Poincaré Map	Lyapunov Exponents	Dimension
Equilibrium point	point		$0 > \lambda_1 \geq \cdots \geq \lambda_n$	0
Periodic / Subharmonic	closed curve	point / closed orbit	$\lambda_1 = 0$ $0 > \lambda_2 \geq \cdots \geq \lambda_n$	1
Two-periodic	torus	closed curve	$\lambda_1 = \lambda_2 = 0$ $0 > \lambda_3 \geq \cdots \geq \lambda_n$	2
K-periodic	K-torus	$(K-1)$-torus	$\lambda_1 = \cdots = \lambda_K = 0$ $0 > \lambda_{K+1} \geq \cdots \geq \lambda_n$	K
Chaotic	Cantor-like	Cantor-like	$\lambda_1 > 0$ $\Sigma_i \lambda_i < 0$	noninteger

0, the only possibility for the Lyapunov exponents of a strange attractor is $(+\ 0\ -)$, that is, $\lambda_1 > 0$, $\lambda_2 = 0$, and $\lambda_3 < 0$. In fourth-order systems, there are two cases[25]

$$(+\ 0\ -\ -): \quad \lambda_1 > 0 \quad \lambda_2 = 0 \quad \lambda_3, \lambda_4 < 0.$$

$$(+\ +\ 0\ -): \quad \lambda_1, \lambda_2 > 0 \quad \lambda_3 = 0 \quad \lambda_4 < 0.$$

The latter case has been termed hyper-chaos [11] since there is expansion in more than one direction. The classification scheme is summarized in Table 1.

VI. Invariant Manifolds of the Poincaré Map

The theory of strange attractors is in its infancy; in fact, there is no general agreement in the research community on what constitutes a strange attractor. One feature that some researchers use as defining characteristic is the transverse intersection of certain invariant manifolds of the Poincaré map.

Consider a fixed point x^* of a two-dimensional Poincaré map $P: \mathbb{R}^2 \to \mathbb{R}^2$. Suppose x^* is a saddle point with characteristic multipliers $|m_1| > 1$, $|m_2| < 1$ and corresponding eigenvectors η_1 and η_2. Associated with the unstable eigenvector η_1 is a curve $W^u(x^*)$ called the *unstable manifold at* x^*. $W^u(x^*)$ is tangent to η_1 at x^* and is invariant under P. Likewise, there is a *stable manifold* $W^s(x^*)$ tangent to the stable eigenvector η_2 at x^* that is also invariant under P. A typical $W^u(x^*)$ and $W^s(x^*)$ are shown in Fig. 16.

It is tempting to think of the invariant manifolds as trajectories, but they are not. Remember that an orbit of the Poincaré map is a sequence of points $\{x_k\}_{k=0}^{\infty}$. A typical orbit starting on the unstable manifold is shown in Fig. 16. The fact that the manifolds are not trajectories opens the possibility of their intersection (at some point other than x^*). Suppose that there is a point $\hat{x} \neq x^*$ such that $\hat{x} \in W^u(x^*)$ and $\hat{x} \in W^s(x^*)$. Since $W^u(x^*)$ and $W^s(x^*)$ are invariant, $\{P^k(\hat{x})\}_{k=-\infty}^{\infty} \subset W^u(x^*)$ and $\{P^k(\hat{x})\}_{k=-\infty}^{\infty} \subset W^s(x^*)$. Thus the existence of one point of intersection implies an infinity of intersections. One possibility is the homoclinic connection of Fig. 17(a) where $W^u(x^*) = W^s(x^*)$. Another is the case of transverse intersections as shown in Fig. 17(b). It is the latter case that interests us since an infinite number of transverse intersections implies a very complicated pattern of stretching and folding of the manifolds near x^*. Stretching and folding are associated with sensitive dependence on initial conditions and, therefore, a transverse intersection of $W^u(x^*)$ with $W^s(x^*)$ is a good indication of chaotic behavior.

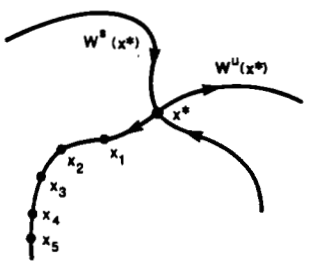

Fig. 16. The stable and unstable invariant manifolds associated with a nonstable fixed point. The sequence of points $\{x_i\}$ represents a typical orbit on the unstable manifold.

[25]As far as we know, the case $(+\ 0\ 0\ -)$ has never been observed.

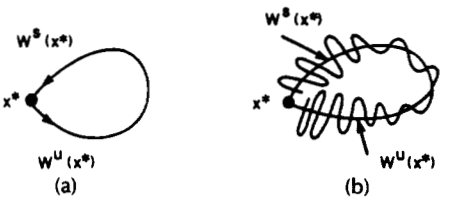

Fig. 17. Two cases of intersecting invariant manifolds. (a) $W^u(x^*) = W^s(x^*)$ (homoclinic connection). (b) $W^u(x^*)$ and $W^s(x^*)$ intersect transversely.

This result is rigorized and generalized to nth-order systems in the Smale–Birkhoff Homoclinic Theorem and is used in Melnikov's Theorem—one of the few ways to prove analytically that sensitive dependence on initial conditions exists [7].

VII. Dimension

In this section, we classify attractors using the concept of dimension. An attractor could be defined to be n-dimensional if, in a neighborhood of every point, it looks like an open subset of $\mathbb{R}^n$ (i.e., it is diffeomorphic to an open subset of $\mathbb{R}^n$). This is how the dimension of a manifold is defined in differential topology. For instance, a limit cycle is one-dimensional since it looks locally like an interval. A torus is two-dimensional since, locally, it resembles an open subset of $\mathbb{R}^2$. An equilibrium point is considered to have zero dimension. The neighborhood of any point of a strange attractor, however, has a fine structure (see Fig. 15) and does not resemble any Euclidean space. Hence, strange attrac-

tors are not manifolds and do not have integer dimension. There are several ways to generalize dimension to the fractional case and four are presented here: capacity, information dimension, correlation dimension, and Lyapunov dimension.

A. Capacity

The simplest type of dimension is *capacity*, also referred to as *fractal dimension*. The idea is as follows. Cover an attractor A with volume elements (spheres, cubes, etc.), each with diameter ϵ. Let $N(\epsilon)$ be the number of volume elements needed to cover A. As ϵ is made smaller, the sum of the volume elements approaches the volume of A. If A is a D-dimensional manifold (D is necessarily an integer), then for ϵ small, the number of volume elements needed to cover A is inversely proportional to ϵ^D, that is, $N(\epsilon) = k\epsilon^{-D}$ for some constant k. The definition of D_{cap} is obtained by solving this equation for D and taking the ϵ-limit

$$D_{cap} := \lim_{\epsilon \to 0} \frac{\ln N(\epsilon)}{\ln (1/\epsilon)}. \tag{38}$$

If the limit does not exist then D_{cap} is undefined.[26] Clearly, for manifolds, D_{cap} is equal to the dimension of the manifold which is an integer; however, for objects that are not manifolds, D_{cap} is usually a noninteger.

Example 1. The unit interval:

Cover the unit interval [0, 1] with volume elements (intervals) of length $\epsilon = 1/3^n$ (Fig. 18(a)). Then $N(\epsilon) = 3^n$. To refine

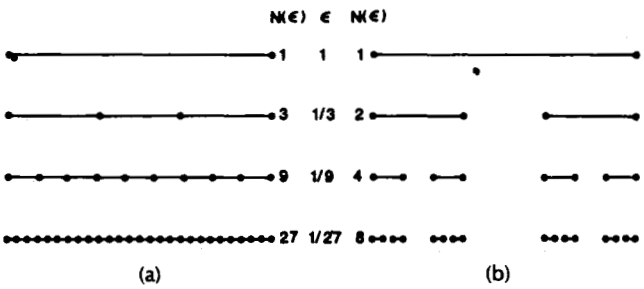

Fig. 18. Two simple examples of capacity. (a) The unit interval. (b) The middle-third Cantor set.

the covering, let $n \to \infty$ to arrive at

$$D_{cap} = \lim_{n \to \infty} \frac{\ln 3^n}{\ln 3^n} = 1. \tag{39}$$

The unit interval has dimension 1 as expected.

Example 2. The middle-third Cantor set:

Remove the middle third of the unit interval leaving the two intervals [0, 1/3] and [2/3, 1]. Remove the middle third of each of these intervals leaving four intervals. Repeat this process *ad infinitum*. The resulting set is called the *middle-third Cantor set*. Cantor sets are useful in the study of Smale horseshoes and they have several interesting properties including fractional dimension and a fine structure similar to that observed in chaotic systems. To show that D_{cap} of this Cantor set is not an integer, choose a covering of intervals with length $\epsilon = 1/3^n$ (Fig. 18(b)). Then $N(\epsilon) = 2^n$ and

$$D_{cap} = \lim_{n \to \infty} \frac{\ln 2^n}{\ln 3^n} = \frac{\ln 2}{\ln 3} = 0.6309 \cdots. \tag{40}$$

Hence, the Cantor set is something more than a point (dimension 0), but something less than an interval (dimension 1).

B. Information Dimension

D_{cap} is a purely metric concept and does not utilize information about the time behavior of the dynamical system. *Information dimension* is a probabilistic type of dimension, defined in terms of the relative frequency of visitation of a trajectory. The setting is the same as for capacity: a covering of $N(\epsilon)$ volume elements each with diameter ϵ. The information dimension D_I is defined by

$$D_I := \lim_{\epsilon \to 0} \frac{\ln S(\epsilon)}{\ln (1/\epsilon)} \tag{41a}$$

where

$$S(\epsilon) := -\sum_{i=1}^{N(\epsilon)} P_i \ln P_i. \tag{41b}$$

P_i is the relative frequency with which a typical trajectory enters the ith volume element of the covering.

Readers familiar with information theory will recognize $S(\epsilon)$ as entropy—the amount of information needed to specify the state of the system to an accuracy of ϵ if the state is known to be on the attractor. Hence, the name information dimension.

Equation (41a) may be rewritten as

$$S(\epsilon) = k\left(\frac{1}{\epsilon}\right)^{D_I} \tag{42}$$

for sufficiently small ϵ. In words, the amount of information needed to specify the state increases inversely with the D_Ith power of ϵ.

C. Correlation Dimension

Another probabilistic type of dimension is the *correlation dimension* D_C defined by

$$D_C := \lim_{\epsilon \to 0} \frac{\ln \sum_{i}^{N(\epsilon)} P_i^2}{\ln \epsilon}. \tag{43}$$

To help interpret the numerator of (43), suppose N points of a trajectory have been gathered either through simulation or from measurements. Define the correlation as

$$C(\epsilon) := \lim_{N \to \infty} \frac{1}{N^2} \{\textit{the number of pairs of points } x_i, x_j \textit{ such that } \|x_i - x_j\| < \epsilon\}. \tag{44}$$

Then

$$D_C = \lim_{\epsilon \to 0} \frac{\ln C(\epsilon)}{\ln \epsilon}. \tag{45}$$

D_C can be easily calculated because $C(\epsilon)$ is easy to estimate as will be shown in Part II.

[26] When the limit exists, the question arises whether another covering (e.g., spheres instead of cubes or, perhaps, a mixture of spheres of different sizes) could result in a different value of D_{cap}. This question cannot be answered adequately in this tutorial. We simply comment that capacity is a special case of Hausdorff dimension and that the definition of Hausdorff dimension implies that if different coverings result in different values of D_{cap}, the minimum value should be used [12].

To show the plausibility of (45), let n_i be the number of points lying in the ith volume element. Then

$$P_i = \lim_{N\to\infty} n_i/N$$

and, since the volume element has diameter ϵ, all the n_i points lie within ϵ of each other forming n_i^2 pairs of points.[27] It follows that

$$C(\epsilon) = \lim_{N\to\infty} \frac{1}{N^2} \sum_i^{N(\epsilon)} n_i^2 \tag{46a}$$

$$= \lim_{N\to\infty} \sum_i^{N(\epsilon)} \frac{n_i^2}{N^2} \tag{46b}$$

$$= \sum_i^{N(\epsilon)} \left\{ \lim_{N\to\infty} \frac{n_i^2}{N^2} \right\} \tag{46c}$$

$$= \sum_i^{N(\epsilon)} P_i^2 \tag{46d}$$

from which (45) follows.

D. Lyapunov Dimension

Let $\lambda_1 \geq \cdots \geq \lambda_n$ be the Lyapunov exponents of a dynamical system. Let j be the largest integer such that $\lambda_1 + \cdots + \lambda_j \geq 0$. The *Lyapunov dimension* D_L as defined by Kaplan and Yorke [13] is

$$D_L := j + \frac{\lambda_1 + \cdots + \lambda_j}{|\lambda_{j+1}|}. \tag{47}$$

In a three-dimensional, chaotic system with Lyapunov exponents λ_+, 0, λ_-

$$D_L = 2 + \frac{\lambda_+}{|\lambda_-|}. \tag{48}$$

For an attractor, $\lambda_+ + \lambda_- < 0$ from which it follows that $2 < D_L < 3$.

For a stable limit cycle, $0 = \lambda_1 > \lambda_2 \geq \cdots \geq \lambda_n$ so $j = 1$ and $D_L = 1$ as expected. Likewise, the Lyapunov dimension of a two-torus is $D_L = 2$. For the chaotic system of Fig. 15(d), the Lyapunov dimension is calculated to be $D_L = 2.13$.

The derivation of (47) is not rigorous and we present a plausibility argument. Consider a hyper-cube C with side ϵ. With the proper change of coordinates, the ith side of C evolves under the flow as $\epsilon e^{\lambda_i t}$ (on the average). Now consider a hyper-cube of side ϵ whose sides all contract at the same rate $\epsilon e^{\lambda_{k+1} t}$ where k is chosen such that $\lambda_{k+1} < 0$ (the λ_i are numbered in decreasing value as before). The number of these cubes it takes to cover C at a given time t is

$$N(t) := \frac{\epsilon e^{\lambda_1 t}}{\epsilon e^{\lambda_{k+1} t}} \cdots \frac{\epsilon e^{\lambda_k t}}{\epsilon e^{\lambda_{k+1} t}} \tag{49a}$$

$$= e^{(\lambda_1 + \cdots + \lambda_k - k\lambda_{k+1})t}. \tag{49b}$$

The sides of C that grow with rates $\lambda_{k+2}, \cdots, \lambda_n$ need not be considered in the limit since they are shrinking with respect to $e^{\lambda_{k+1} t}$.

The capacity is approximated by

$$D(k) = -\lim_{t\to\infty} \frac{\ln N(t)}{\ln (\epsilon e^{\lambda_{k+1} t})} \tag{50a}$$

$$= k - \frac{\lambda_1 + \cdots + \lambda_k}{\lambda_{k+1}}. \tag{50b}$$

It can be shown that $k = j$ yields the lowest value of $D(k)$ so define [28]

$$D_L := D(j) = j - \frac{\lambda_1 + \cdots + \lambda_j}{\lambda_{j+1}} \tag{51a}$$

$$= j + \frac{\lambda_1 + \cdots + \lambda_j}{|\lambda_{j+1}|} \tag{51b}$$

to complete the plausibility argument.

E. Discussion of Dimension

As Table 1 shows, the classification of attractors by their dimension is quite straightforward. A simple attractor (equilibrium point, limit cycle, torus) has integer dimension; strange attractors have fractional dimension.

An attractor of a Poincaré map with dimension D corresponds to an attractor of the underlying flow with dimension $D + 1$. For example, if the attractor of the Poincaré map is a closed curve (dimension 1), the attractor of the flow is a torus (dimension 2).

Given the different definitions of dimension, it is natural to ask what relationship they bear to one another. Are they equivalent? Is one more useful than another?

Capacity is the simplest and is useful for illustrating what a frational dimension means. It, however, treats the attractor as a static geometrical object ignoring the fact that there is a dynamical flow defined on it (and defining it). In a simulation or experiment, the attractor is not seen directly, only typical trajectories over finite time periods are observed. Thus capacity is of questionable use in a practical setting. The three other types of dimension utilize probabilistic concepts and are more suited to experiments and simulations.

Information dimension weights a volume element according to how often a trajectory is found in it. Volume elements that are visited infrequently have little influence on D_I. Thus one would expect (and it can be proved) that $D_I \leq D_{cap}$ with equality if all the volume elements have the same relative frequency. This argument also points out a drawback of capacity in experimental settings. For an accurate calculation of D_{cap}, the system must run long enough to guarantee that the trajectory has visited nearly every volume element. The required time interval and the resulting amount of data is often prohibitively large.

Correlation dimension, a probabilistic type of dimension, is superior to capacity for the same reasons as D_I. Currently, there appears to be no reason to prefer D_I over D_C. It can be shown that $D_C \leq D_I \leq D_{cap}$ [14].

As is obvious from the definition, Lyapunov dimension is somewhat different from the other three. In fact, it is not even clear that D_L is actually a dimension. It was originally conjectured that $D_L = D_{cap}$ as the plausibility argument is designed to show. However, since Lyapunov exponents are probabilistic in nature and D_{cap} is not, the conjecture was changed to $D_L = D_I$. Numerical simulations do not appear to contradict this conjecture, but analytical examples exist where $D_L \neq D_I$ [14]. These examples, however, are not structurally stable and if perturbed, the relationship $D_L = D_I$ does hold. The exact relationship between D_L *and* D_I (and the other dimensions as well) is an active research topic.

Calculation of D_L requires calculation of all the positive

[27] Note that x_i, x_i is counted as a pair and for $i \neq j$, x_i, x_j is treated as a different pair from x_j, x_i.

[28] Remember that if two different coverings result in different capacities, the minimum value should be used.

Lyapunov exponents and some of the negative ones. The Lyapunov exponents are easy to find by simulation since the variational equation can be solved using integration routines. We know of no way to find all the Lyapunov dimensions experimentally since current techniques cannot calculate the negative Lyapunov exponents.

VIII. Reconstruction of Attractors

In this section, we pesent a remarkable fact that allows a strange attractor to be reconstructed from a sampled time waveform of just one component of the state. This is a useful technique in experimental settings. If data are gathered from measurements of a physical system, only one state needs to be measured, cutting instrumentation and data storage costs. For an infinite-order system or in finite systems where one or more of the states cannot be measured directly, reconstruction may be the only way to observe the attractor.

The reconstruction function F is defined as follows. Let the attractor A be contained in a compact[29] manifold M of dimension N. Define $F: M \to \mathbb{R}^{2N+1}$ as

$$F(x) := [\phi_0^j(x)\ \phi_\tau^j(x)\ \cdots\ \phi_{2N\tau}^j(x)]^T \tag{52}$$

where $\phi_t^j(x)$ is the jth component of the trajectory (j is arbitrary) and $\tau > 0$ is the sampling period, also arbitrary. Then, generically,[30] F is an *embedding*; that is, F diffeomorphically maps M onto some compact N-dimensional submanifold M' of $\mathbb{R}^{2N+1}$.

The implication is that given a time series $\{y_k\}_{k=0}^K$ where $y_k := \phi_{k\tau}^j(x)$ is the jth component of a trajectory that lies on A, the sequence of points

$$\begin{gathered}
[y_0\ y_1\ \cdots\ y_{2N}]^T \\
[y_1\ y_2\ \cdots\ y_{2N+1}]^T \\
\vdots \\
[y_i\ y_{i+1}\ \cdots\ y_{i+2N}]^T \\
\vdots \\
[y_{K-2N}\ y_{K-2N+1}\ \cdots\ y_K]^T
\end{gathered} \tag{53}$$

lies on a diffeomorphic copy of A.

Several examples of reconstructed attractors are shown in Fig. 19. The reconstructed versions are definitely different from the originals, but can be seen to share the same qualitative features. Moreover, it can be shown that the dimension of the reconstruction is equal to the dimension of the original [15].

At first glance, it seems preposterous that one component of a trajectory carries enough information to reconstruct the entire attractor and, even if it did, that the simple function F would accomplish the feat. It is clear that F is differentiable due to differentiability with respect to the initial condition. What is surprising is that $F^{-1}: M' \to M$ exists. To show that invertibility is actually quite reasonable, we present two plausibility arguments.

[29] In Euclidean space, a *compact* set is one that is closed and bounded.

[30] In this setting, the term *generic* is difficult to define precisely. It is sufficient to think of *property P is generic* as meaning *for randomly chosen parameters the system will exhibit property P with probability 1.*

Plausibility Argument 1:

This argument suggests that F is one-to-one by demonstrating the invertibility of a very similar function.

Define $\hat{F}: \mathbb{R}^n \to \mathbb{R}^n$ by

$$\hat{F}(x) := [\phi_0^j(x)\ \phi_\tau^j(x)\ \cdots\ \phi_{(n-1)\tau}^j(x)]^T \tag{54}$$

for some $\tau > 0$. We will argue that $\hat{F}(x)$ identifies $\phi_t(x)$ uniquely and, since there is a one-to-one correspondence between trajectories and initial conditions, $\hat{F}$ is invertible.

To identify uniquely a trajectory of an nth-order system, n independent pieces of information are needed. This information may be specified in several ways. The three we will discuss are

i) Give the initial condition, $x = \phi_0(x)$.
ii) Give the first $(n-1)$ derivatives of one of the states, $[\phi_0^j(x)\ D_t\phi_0^j(x)\ \cdots\ D_t^{n-1}\phi_0^j(x)]^T$.
iii) Give n samples of one of the states, $\hat{F}(x) = [\phi_0^j(x)\ \phi_\tau^j(x)\ \cdots\ \phi_{(n-1)\tau}^j(x)]^T$.

Method i) always works and is the standard way of specifying a trajectory. Methods ii) and iii) do not work if the system is insufficiently coupled. For instance, ii) and iii) fail for

$$\begin{bmatrix} \dot{x} \\ \dot{y} \end{bmatrix} = \begin{bmatrix} \alpha & \epsilon \\ \epsilon & \beta \end{bmatrix} \begin{bmatrix} x \\ y \end{bmatrix} \tag{55}$$

when $\epsilon = 0$. However, for $\epsilon \neq 0$—the generic case—they do work.

In addition, method iii) fails when there is periodicity in the system that is related to τ. For instance, if the trajectory is periodic with period T, then $\phi_{kT}^j(x) = \phi_{(k+1)T}^j(x)$ for $k = 0, 1, \cdots$. If $\tau = T$, then iii) does not supply n independent pieces of information and, therefore, does not uniquely determine a trajectory. However, with a slight perturbation of τ, the problem disappears and, generically, $\hat{F}$ is invertible.

The preceding argument shows that F is generically one-to-one if $n \leq 2N + 1$. To show invertibility for any n, we resort to some ideas from differential topology.

Plausibility Argument 2:

A classic result of differential topology is Whitney's Theorem: If M is an N-dimensional manifold, then there exists an embedding $f: M \to \mathbb{R}^{2N}$.

For example, the circle can be embedded in $\mathbb{R}^2$ (Fig. 20(a)), but not in $\mathbb{R}$. While Whitney's Theorem guarantees M can be embedded in $\mathbb{R}^{2N}$, it is of little use in showing that F is an embedding.

Modified version of Whitney's Theorem [15]: If M is compact and $f: M \to \mathbb{R}^{2N+1}$ is twice continuously differentiable, then, generically, f is an embedding.

As an example, let $f: S \to \mathbb{R}^2$ be a continuously differentiable map that transforms the circle into a figure eight (Fig. 20(b)). f is not an embedding because it is one-to-one. Furthermore, no small perturbation of f can make it one-to-one. But if the dimension of the range is increased to three, almost every perturbation produces a one-to-one map $\hat{f}$: $S \to \mathbb{R}^3$ (Fig. 20(c)) and, therefore, the property of being one-to-one is generic.

The dimensions of the domain and range of the reconstruction map F satisfy the modified theorem and F is differentiable due to differentiability of trajectories with

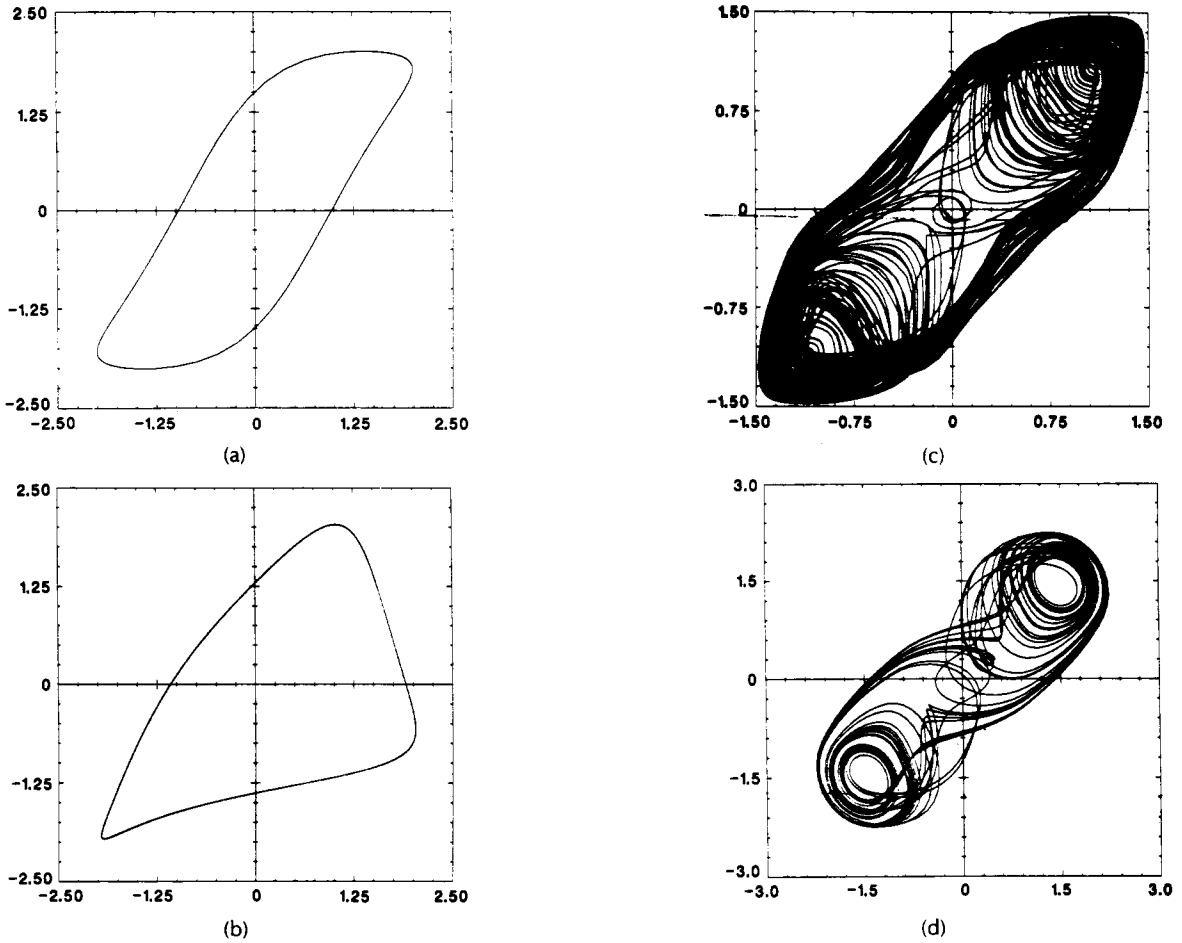

Fig. 19. Reconstructed attractors. (a) van der Pol limit cycle (Fig. 3). (b) van der Pol two-periodic solution (Poincaré map) (Fig. 13). (c) Duffing's equation (Fig. 6(a)). (d) Double scroll equation (Fig. 6(d)).

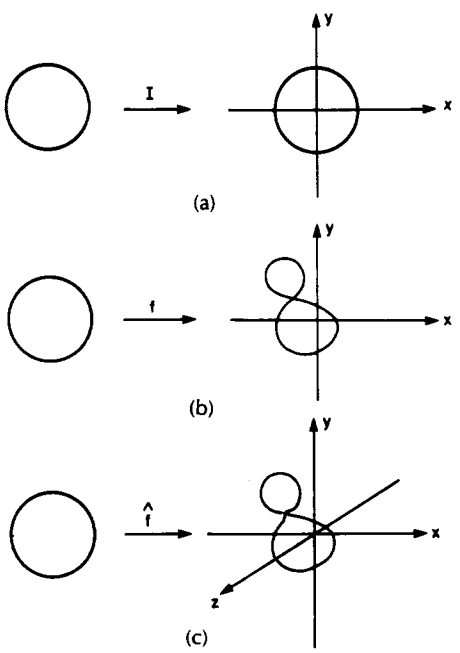

Fig. 20. Maps of the circle into Euclidean space. (a) A map of the circle into $\mathbb{R}^2$ that is an embedding. (b) A differentiable map $f: S \to \mathbb{R}^2$ that is not an embedding because it is not one-to-one. (c) If the range of f is changed to $\mathbb{R}^3$, then a slight perturbation makes it one-to-one and, therefore, an embedding.

respect to the initial condition. Hence, F is generically an embedding.

This argument guarantees that $\mathbb{R}^{2N+1}$ is always sufficient to reconstruct an attractor. It is quite possible that a reconstruction space with dimension less than $2N + 1$ can be used. For example, as the first plausibility argument shows, if $n < 2N + 1$, $\mathbb{R}^n$ is sufficient.

There are two questions remaining. How is τ picked and what happens if N is not known?

Almost every τ will work, but there are three practical limitations. If τ is too small, then $\phi^j_{k\tau}(x) \approx \phi^j_{(k+1)\tau}(x)$ and the reconstructed attractor is restricted to the diagonal of the reconstruction space. If τ is too large and the system is chaotic, then $\phi^j_{k\tau}(x)$ and $\phi^j_{(k+1)\tau}(x)$ are uncorrelated (to working precision), and the structure of the reconstructed attractor disappears. If τ is close to some periodicity in the system, the component at that period will be under-represented in the reconstruction. This effect is similar to the stroboscopic action of the nonautonomous Poincaré map which freezes a particular periodic component. Fig. 21 shows a reconstructed attractor for various values of τ.

If N is not known, it can be found as follows. Let n_r be the dimension of the reconstruction space $\mathbb{R}^{n_r}$. Set $n_r = 1$ and calculate the dimension D_C, say, of the reconstructed attractor. Repeat this calculation, incrementing n_r each time, until D_C does not change any more. This final D_C is the proper value of the correlation dimension, and the lowest n_r yield-

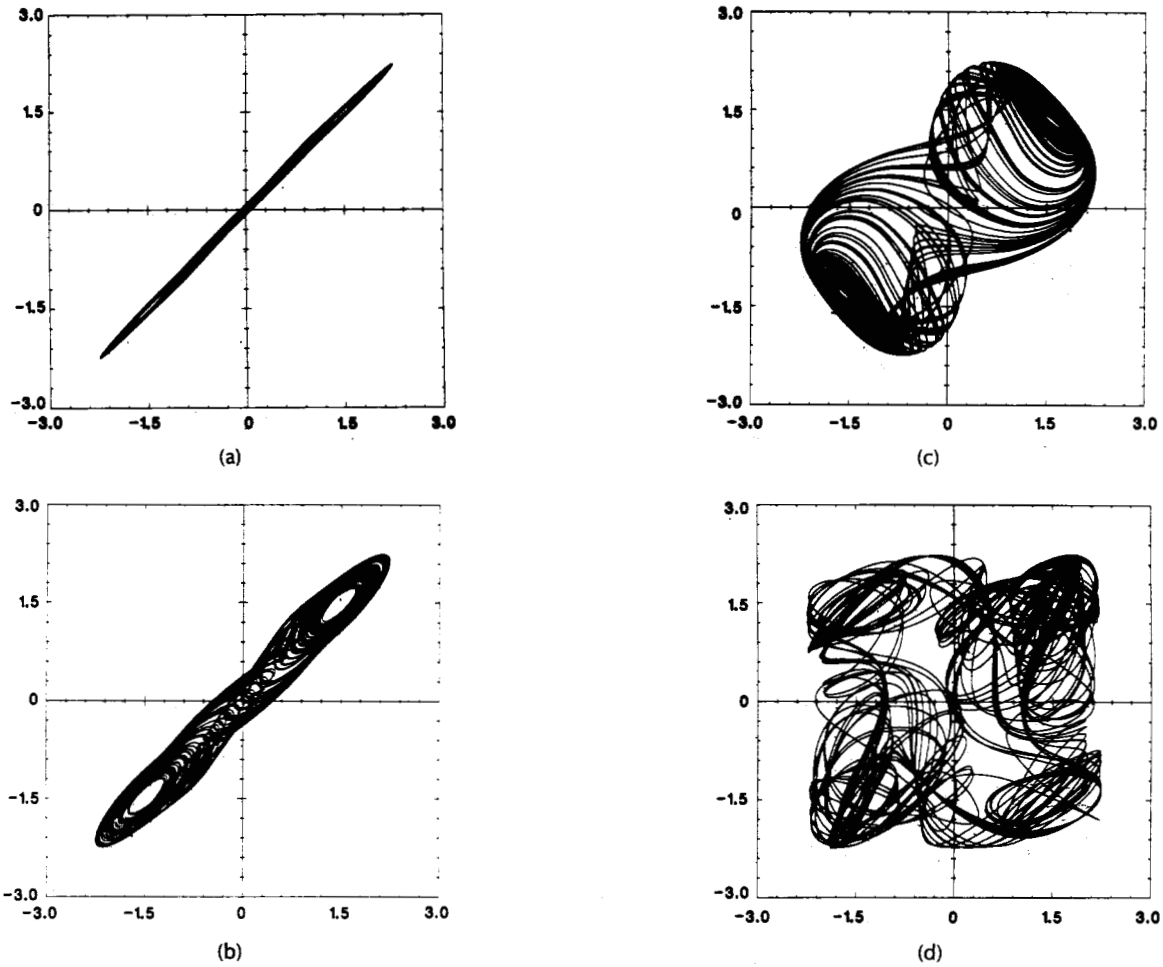

Fig. 21. Several reconstructions of the double scroll attractor (Fig. 6(d)) for various values of τ. (a) $\tau = 0.05$. (b) $\tau = 0.25$. (c) $\tau = 1.25$. (d) $\tau = 6.25$.

ing this value is the minimal dimension of the reconstruction space. This technique has been used successfully on infinite-order systems. [14].

Part II: Practical Algorithms

IX. Introduction

All the analysis techniques presented in Part I share one important feature: there exist simple numerical algorithms to implement them. In this part of the tutorial, we present numerical techniques for locating equilibrium points and periodic solutions, and for calculating characteristic multipliers, Lyapunov exponents, and correlation dimension. We also introduce a new algorithm for calculating the invariant manifolds of a two-dimensional Poincaré map. All these algorithms are included in the INSITE nonlinear systems simulation toolkit [16].

A. The Variational Equation

The algorithms for locating limit cycles and calculating Lyapunov exponents require the solution of the variational equation (31). $\Phi_t(x)$ is most easily calculated by appending the variational equation to the equations describing the dynamical system

$$\begin{Bmatrix} \dot{x} \\ \dot{\Phi} \end{Bmatrix} = F(x, \Phi, t) := \begin{Bmatrix} f(x, t) \\ Df(x, t)\Phi \end{Bmatrix} \qquad \begin{Bmatrix} x(t_0) \\ \Phi_{t_0} \end{Bmatrix} = \begin{Bmatrix} x_0 \\ I \end{Bmatrix}. \tag{56}$$

Integrate this $(n^2 + n)$-dimensional system to find $\phi_t(x_0, t_0)$ and $\Phi_t(x_0, t_0)$ simultaneously.

X. Locating Limit Sets

The obvious way to locate a steady-state solution using computer simulations is what we call the *brute-force* method: integrate the dynamical system until the transient has died out. The brute-force approach has the advantage of simplicity, and it is general in that it applies to periodic, quasi-periodic, and chaotic solutions, as well as equilibrium points. It suffers from several drawbacks, the most severe of which is long simulation times. Lightly damped systems have long-lived transients and result in unacceptably long simulations. A related problem is that there is no reliable way to detect the end of the transient. More than once, a trajectory which we had decided was chaotic turned out—after further simulation—to be a chaotic transient of a periodic steady state.

The brute-force method also suffers from the fact that it cannot locate unstable or nonstable limit sets. The ability to locate unstable equilibrium points and periodic solutions is crucial to understanding the bifurcation behavior of nonlinear systems.

More sophisticated techniques—useful for finding equilibrium points and periodic solutions—utilize the *Newton-Raphson* algorithm. Consider a function $H: \mathbb{R}^n \to \mathbb{R}^n$ with a zero at x^* (i.e., $H(x^*) = 0$). Newton-Raphson attempts to calculate x^* by iterating from an initial guess $x^{(0)}$ using the relation[31]

$$x^{(i+1)} = x^{(i)} - DH(x^{(i)})^{-1} H(x^{(i)}). \tag{57}$$

This expression is obtained by approximating the equation $y^{(i)} = H(x^{(i)})$ by its linearization

$$\Delta y^{(i)} = DH(x^{(i)}) \Delta x^{(i)} \tag{58}$$

where $\Delta y^{(i)} := y^{(i+1)} - y^{(i)}$, and $\Delta x^{(i)} := x^{(i+1)} - x^{(i)}$. We want to choose $x^{(i+1)}$ such that $y^{(i+1)} = 0$. Therefore

$$-y^{(i)} = DH(x^{(i)})(x^{(i+1)} - x^{(i)}) \tag{59}$$

from which (57) follows. Of course, since (58) is only an approximation, it is not expected that $H(x^{(i+1)}) = 0$, but it is hoped that successive iterations of (57) yield a better and better approximation to x^*.

Pseudo-code for a practical implementation of the Newton-Raphson algorithm is shown in Fig. 22.

```
begin NewtonRaphson
    choose x[0], E_r, E_a, ε, and i_max
    set i = 0
    set x[] = x[0]
    repeat
        set i = i + 1
        if i > i_max then
            no convergence—exit
        set y[] = H(x[])
        solve DH(x[])z[] = y[] for z[]
        if DH(x[]) is ill-conditioned then
            restart with new x[0]
        set x[] = x[] - z[]
    until ||z[]|| < E_r||x[]|| + E_a and H(y[]) < ε
    output x[]
end NewtonRaphson
```

Fig. 22. Pseudo-code for the Newton-Raphson algorithm. Brackets indicate a variable is a vector (i.e., an array).

Comments:

i) The Newton-Raphson algorithm requires the Jacobian $DH(x^{(i)})$. In practice, $DH(x^{(i)})$ is never inverted. Let $y^{(i)} := H(x^{(i)})$ and $z^{(i)} := DH(x^{(i)})^{-1} y^{(i)}$. Then $x^{(i+1)} = x^{(i)} - z^{(i)}$. $z^{(i)}$ is found by solving the linear system of equations $H(x^{(i)})z^{(i)} = 0$ using standard algorithms such as those supplied in LINPACK [17]. If $DH(x^{(i)})$ is singular (or nearly so), the algorithm must be restarted with a new $x^{(0)}$.

ii) The obvious convergence test for $x^{(i)}$ is

$$\|x^{(i+1)} - x^{(i)}\| < \epsilon. \tag{60}$$

However, this test is sensitive to changes in the scaling of $x^{(i)}$ and should be replaced by a testing scheme that uses relative and absolute error tolerances, E_r and E_a

$$\|x^{(i+1)} - x^{(i)}\| < E_r \|x^{(i)}\| + E_a. \tag{61}$$

This test protects against scaling problems and is equivalent to (60) when $E_r = 0$. In critical circumstances, the error test can be further refined by performing the test separately on each component of x or by weighting the components according to their importance.

iii) In general, a relative/absolute error test cannot be used to check that $H(x^{(i)})$ is approximately zero so a simple absolute test is used: $\|H(x^{(i)})\| < \epsilon$. In the special case where $H(x) = H_1(x) + \cdots + H_p(x)$ is the sum of p functions, the relative/absolute test

$$\|H(x^{(i)})\| < E_r(\|H_1(x)\| + \cdots + \|H_p(x)\|) + E_a \tag{62}$$

should be used.

iv) Convergence of the Newton-Raphson algorithm is guaranteed only if $x^{(0)}$ is sufficiently close to x^* [18]. If it is not, then the algorithm may not converge. However, if the Newton-Raphson algorithm does converge, the convergence is very quick once $x^{(i)}$ gets close to x^*.

A. Locating Equilibrium Points

Equilibrium points are the zeros of the vector field f and as long as Df is available they can be calculated by applying the Newton-Raphson algorithm directly to $H(x) := f(x)$. The stability of the equilibrium point x_{eq} is determined by the eigenvalues of $Df(x_{eq})$. The eigenvalues may be calculated using standard algorithms such as those found in EISPACK [19].

B. Locating Periodic Solutions

The Newton-Raphson algorithm may be applied to the problem of locating periodic solutions as well as equilibrium points. In this application, it is often referred to as the *shooting method*. As usual, we treat the nonautonomous and autonomous cases separately.

1) Nonautonomous Shooting Method: Periodic solutions correspond to fixed points of the Poincaré map $x^* = P(x^*)$. To apply Newton-Raphson, define $H(x) := P(x) - x$. x^* is a fixed point of P if and only if it is a zero of H.

The formulas for the key computational steps in the Newton-Raphson algorithm are

$$y^{(i)} = \phi_{T+t_0}(x^{(i)}, t_0) - x^{(i)} \tag{63a}$$

and

$$DH(x^{(i)}) = \Phi_{T+t_0}(x^{(i)}, t_0) - I \tag{63b}$$

both of which are calculated easily using integration routines. If one is interested in locating a Kth-order subharmonic, simply replace T by KT in (63).

2) The Autonomous Shooting Method: The autonomous case is more difficult since the period is not known beforehand. We present three different methods.

Method 1:

This is the most obvious approach and is a direct generalization of the nonautonomous shooting method. Pick a cross section Σ and then use Newton-Raphson to locate a fixed point of the one-sided Poincaré map defined by Σ. This approach is straightforward, but suffers from the drawback that one must know beforehand that the limit cycle intersects Σ. It is also relatively difficult to program since the point where the trajectory intersects Σ must be located.

The next two methods use Newton-Raphson by realizing that limit cycles correspond to zeros of the map

$$H(x, T) := \phi_T(x) - x. \tag{64}$$

[31] In this section, a superscript enclosed in parentheses indicates the iteration count.

To apply Newton-Raphson, linearize $H(x, T)$

$$\Delta y^{(i)} = D_x H(x^{(i)}, T^{(i)})\Delta x^{(i)} + D_T H(x^{(i)}, T^{(i)})\Delta T^{(i)} \quad (65a)$$

$$= (\Phi_{T^{(i)}}(x^{(i)}) - I)\Delta x^{(i)} + f(\phi_{T^{(i)}}(x^{(i)}))\Delta T^{(i)} \quad (65b)$$

where $\Delta x^{(i)} := x^{(i+1)} - x^{(i)}$, $\Delta y^{(i)} := y^{(i+1)} - y^{(i)}$, and $\Delta T^{(i)} := T^{(i+1)} - T^{(i)}$.

Given $x^{(i)}$, $y^{(i)}$, and $T^{(i)}$, we want to choose $x^{(i+1)}$ and $T^{(i+1)}$ such that $y^{(i+1)} = 0$. Therefore, the Newton-Raphson iteration is given by

$$-y^{(i)} = \Phi_{T^{(i)}}(x^{(i)})(x^{(i+1)} - x^{(i)}) + f(\phi_{T^{(i)}}(x^{(i)}))(T^{(i+1)} - T^{(i)}) \quad (66)$$

which is a system of n equations in the $(n + 1)$ unknowns $x^{(i+1)}$ and $T^{(i+1)}$. One more constraint must be found to make the system of equations uniquely solvable, and this is how Methods 2 and 3 differ.

Method 2 [20]:

At every iteration, fix one component of $x^{(i)}$ thereby reducing the number of unknowns by one. Which particular component is chosen varies from iteration to iteration. A control scheme is presented in [20] as well as the resulting equations for the Newton-Raphson iteration and an expression for the Jacobian. This approach is simpler to program than Method 1, but more difficult than Method 3.

Method 3 [21]:

In this method, the correction term $\Delta x^{(i)}$ is restricted to be orthogonal to the trajectory

$$f(x^{(i)})^T \Delta x^{(i)} = 0. \quad (67)$$

This constraint results in a system of $(n + 1)$ equations in $(n + 1)$ unknowns

$$\begin{bmatrix} -y^{(i)} \\ 0 \end{bmatrix} = \begin{bmatrix} \Phi_{T^{(i)}}(x^{(i)}) - I & f(\phi_{T^{(i)}}(x^{(i)})) \\ f(x^{(i)})^T & 0 \end{bmatrix} \begin{bmatrix} x^{(i+1)} - x^{(i)} \\ T^{(i+1)} - T^{(i)} \end{bmatrix} \quad (68)$$

which can be iterated in the typical Newton-Raphson fashion.

Which of the three methods is best is not clear. Method 3 is the easiest to program while Method 1 is the hardest. Methods 2 and 3 run the risk of converging to an equilibrium point instead of a limit cycle and though this occurrence is easily detected, it is a nuisance. On the other hand, Method 1 never converges to an equilibrium point except in the unlikely event that an equilibrium point lies on Σ.

All three methods rely on the Newton-Raphson algorithm and, therefore, can be sensitive to the initial guess. How sensitive depends on the system under study. Stable limit cycles are usually the least sensitive. Running the system in reverse time can reduce the sensitivity for unstable systems, but usually has little effect for nonstable limit cycles. In any event, the shooting method is most effective when one knows that a limit cycle exists and its approximate location and period.

All three methods require the calculation of $\Phi_{T^{(i)}}(x^{(i)})$ which, upon convergence, is approximately equal to $\Phi_T(x^*)$ and from which the characteristic multipliers can be obtained using EISPACK.

C. Locating Quasi-Periodic Solutions

Locating two-periodic behavior is equivalent to locating an invariant closed curve of the Poincaré map. Some work has been done in this area and the interested reader is referred to [22].

Frequency-domain techniques are also available to tackle this problem [23].

D. Locating Chaotic Solutions

We know of no algorithms for the location of chaotic limit sets other than brute-force integration.

XI. Calculation of the Invariant Manifolds of a Two-Dimensional Poincaré Map

Consider a nonstable fixed-point (saddle-point) x^* of a two-dimensional Poincaré map $P: \mathbb{R}^2 \to \mathbb{R}^2$. Let the characteristic multipliers be $|m_1| > 1$ and $|m_2| < 1$ with corresponding eigenvectors η_1 and η_2. It is our goal to approximate the stable and unstable manifolds $W^s(x^*)$ and $W^u(x^*)$ associated with x^*.

Removal of x^* from $W^u(x^*)$ and $W^s(x^*)$ creates four half-manifolds: $W^{u+}(x^*)$, $W^{u-}(x^*)$, $W^{s+}(x^*)$, and $W^{s-}(x^*)$. As Fig. 23 shows, $W^{u+}(x^*)$ corresponds to the half-manifold tangent to η_1 and $W^{u-}(x^*)$ to the half-manifold tangent to $-\eta_1$. Similar definitions hold for $W^{s+}(x^*)$ and $W^{s-}(x^*)$ with respect to η_2.

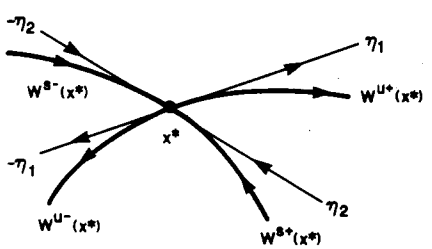

Fig. 23. The four half-manifolds associated with a nonstable equilibrium point.

The algorithms presented here calculate $W^{u+}(x^*)$ for the case $m_1 > 1$. They can be applied directly to find $W^{u-}(x^*)$ by substituting $-\eta_1$ for η_1. The stable half-manifolds can be calculated by running the system in reverse time for they then become the unstable manifolds. If $m_1 < -1$, a point on $W^u(x^*)$ bounces back and forth from $W^{u+}(x^*)$ to $W^{u-}(x^*)$ under repeated applications of P and, therefore, the half-manifolds are not invariant. However, the half-manifolds are invariant with respect to the twice-iterated map, and therefore, can be found by applying the algorithms to P^2. This technique treats x^* as a closed orbit of period two with characteristic multipliers m_1^2 and m_2^2.

Let $\bar{x} \in W^{u+}(x^*)$ be a point on the half-manifold and let $\overline{W} \subset W^u(x^*)$ be the set of points on the half-manifold between $\bar{x}$ and $P(\bar{x})$. Then, assuming $m_1 > 1$, $W^{u+}(x^*)$ is the union

$$\bigcup_{i=-\infty}^{\infty} P_i(\overline{W})$$

of all the forward and reverse iterates of the submanifold $\overline{W}$ and, therefore, determining $W^{u+}(x^*)$ is equivalent to determining $\overline{W}$.

A good $\overline{W}$ can be found by choosing $\bar{x}$ such that it lies on the unstable eigenvector, that is, $\bar{x} = x^* + \alpha\eta_1$ for some small $\alpha > 0$. Near x^*, $P(x)$ can be approximated by $x^* + DP(x^*) \cdot$

$(x - x^*)$. It follows that $P(\bar{x}) \approx x^* + \alpha m_1 \eta_1$ and that $\overline{W}$ is approximated by the line segment connecting $\bar{x}$ and $P(\bar{x})$

$$\overline{W} = \{x | x = x^* + \alpha m \eta_1, 1 \leq m < m_1\}. \quad (69)$$

Given α, the standard method for calculating $W^{u+}(x^*)$ is shown in Fig. 24. Take N uniformly spaced points on $\overline{W}$

$$\bar{x}_i = x^* + \left(1 + \frac{m_1 - 1}{N}(i - 1)\right)\alpha\eta_1, \quad i = 1, \cdots, N \quad (70)$$

where N is some large integer, typically around 100. Repeatedly apply the Poincaré map to these points to obtain a set

```
begin SimpleHalfManifold
    choose α, N, n_iter
    for i from 1 to N
        set x[i] = x* + (1 + (m1 - 1)(i - 1)/N)αη1
        output x[i]
    for j from 1 to n_iter
        for i from 1 to N
            set x[i] = P(x[i])
            output x[i]
end SimpleHalfManifold
```

Fig. 24. Pseudo-code for the typical method of calculating the half-manifold $W^{u+}(x^*)$.

of points contained in $W^{u+}(x^*)$. If N is chosen large enough, the points give a good indication of the unstable half-manifold. This method is very simple to understand and to program, but possesses two flaws.

First, how is α chosen? Too large a value implies that the initial segment $\overline{W}$ does not lie on $W^{u+}(x^*)$. Too small a value results in long integration times and increases the chance of the accumulated numerical error affecting the result.

Second, even though $\bar{x}_i$ *and* $\bar{x}_{i+1}$ are near one another, their iterates, $P^j(\bar{x}_i)$ and $P^j(\bar{x}_{i+1})$, may be quite far apart resulting in a poor approximation of $W^{u+}(x^*)$. This stretching is especially common in chaotic systems.

Suppose that for an accurate estimation of $W^{u+}(x^*)$, it is required that none of the distances $\| P^j(\bar{x}_i) - P^j(\bar{x}_{i+1}) \|$ exceed $\epsilon > 0$ and that this constraint is satisfied for $j < j'$ but not for $j = j'$. With this algorithm, the only way to achieve the desired tolerance for $j = j'$ is to increase N to some value N'. This increase, however, leads to increased computation since $(N' - N)$ additional points must be carried through the first $(j' - 1)$ iterations even though they are only needed for the j'th iteration.

We now introduce a new algorithm which overcomes both these objections. The algorithm varies N from iteration to iteration and from point to point, and it also employs a scheme for calculating α. Pseudo-code for the algorithm is presented in Fig. 25.

A. Calculation of α

In the α-selection algorithm, *FindAlpha*, it is assumed that the unstable eigenvector is normalized to $\| \eta_1 \| = 1$. The algorithm starts with $\alpha^{(0)} = 1$ and halves α until an acceptable value is found or some minimum α is reached. $\alpha^{(i)}$ is deemed acceptable if the linearized map.

$$P_L(\bar{x}^{(i)}) := x^* + DP(x^*)(\bar{x}^{(i)} - x^*) \quad (71a)$$

$$= x^* + \alpha^{(i)} m_1 \eta_1 \quad (71b)$$

is a good approximation to $P(\bar{x}^{(i)})$ for $\bar{x}^{(i)} = x^* + \alpha^{(i)}\eta_1$ where $\alpha^{(i)} = 1/2^i$ is the current value of α. A typical situation is shown in Fig. 26. As in the Newton–Raphson algorithm, a relative/

```
begin HalfManifold
    choose ε, n_pts
    call Initialize
    set i = 1
    while i ≤ n_pts
        if ||Px[2] - Px[1]|| < ε then
            call Accept
            set i = i + 1
        else
            call Interpolate
end HalfManifold

begin Initialize
    call FindAlpha
    set n_x = n_Px = 2
    set x[1] = x* + αη1
    set Px[1] = x[2] = P(x[1])
    set Px[2] = P(x[2])
end Initialize

begin FindAlpha
    choose α_min, E_r, E_a
    set α = 2.0
    repeat
        set α = α/2.0
        if α < α_min
            return α_min
        set x[] = x*[] + αη1[]
        set P_L x[] = x*[] + α m1 η1[]
    until ||P_L x[] - P(x[])|| < E_r ||P_L x[]|| + E_a
    return α
end FindAlpha

begin Accept
    output Px[1]
    for i from 1 to n_x
        set x[i] = x[i + 1]
    set x[n_x] = Px[1]
    set n_Px = n_Px - 1
    for i from 1 to n_Px
        set Px[i] = Px[i + 1]
    if n_Px = 1 then
        set Px[2] = P(x[2])
        set n_Px = 2
end Accept

begin Interpolate
    set n_x = n_x + 1
    for i from 3 to n_x
        set x[i] = x[i - 1]
    set x[2] = (x[1] + x[3])/2.0
    set n_Px = n_Px + 1
    for i from 3 to n_Px
        set Px[i] = Px[i - 1]
    set Px[2] = P(x[2])
end Interpolate
```

Fig. 25. Pseudo-code for a more robust method to calculate the half-manifold $W^{u+}(x^*)$.

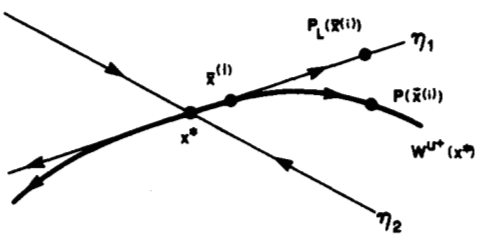

Fig. 26. A typical situation showing the relationship between $\bar{x}^{(i)}$, $P(\bar{x}^{(i)})$, and $P_L(\bar{x}^{(i)})$.

absolute error scheme protects this algorithm from scaling problems.

We have found that for m_1 near 1, $W^{u+}(x^*)$ usually possesses a fairly high degree of curvature and a relatively small value of α is selected, but if $m_1 \gg 1$, $W^{u+}(x^*)$ is virtually straight near x^* and a larger α can be used.

B. Calculation of the Invariant Manifold

Given a proper value of α, this algorithm produces a sequence of points $\{y_i\}_{i=1}^{n_y}$ that lies on $W^{u+}(x^*)$ such that for $1 \leq i < n_y$, $\| y_{i+1} - y_i \| < \epsilon$ and y_{i+1} lies further along the half-manifold than y_i (in the sense of arc-length mea-

sured from x^*). The algorithm uses two arrays $x[\ ]$ and $Px[\ ]$. $x[\ ]$ contains n_x points and defines a portion of $W^{u+}(x^*)$ that is one iteration long (i.e., $x[n_x] = P(x[1])$). $x[\ ]$ may be thought of as a window that slides along $W^{u+}(x^*)$ as the algorithm progresses. $Px[\ ]$ is the Poincaré map of $x[\ ]$, that is, $Px[i] = P(x[i])$ for $i = 1, \cdots, n_x$ (Fig. 27(a)).

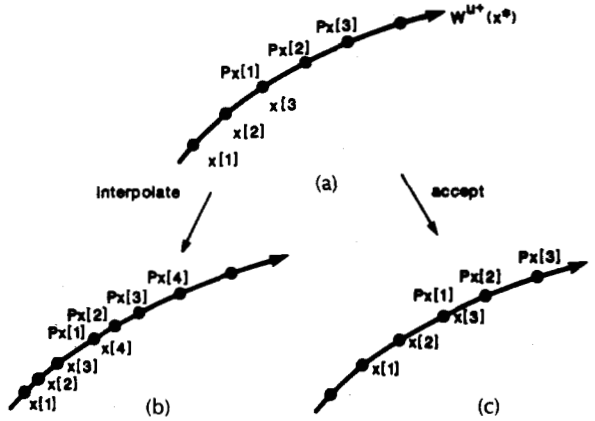

Fig. 27. Examples of the $x[\ ]$ and $Px[\ ]$ arrays. (a) The array $x[\ ]$ contains points that lie on a subset of $W^{u+}(x^*)$ that is one iteration long. $Px[\ ]$ is the Poincaré map of $x[\ ]$. (b) The interpolation process. (c) The acceptance process.

The algorithm checks whether $\|Px[2] - Px[1]\| < \epsilon$. If not, the resolution of $Px[\ ]$ must be increased. This is accomplished by interpolating a value midway between $x[1]$ and $x[2]$ and applying P to the resulting point. More precisely, the $x[\ ]$ array is expanded by shifting all entries except $x[1]$ one to the right and setting $x[2] = (x[1] + x[3])/2$. The $Px[\ ]$ array is then expanded in a like manner, $Px[2]$ is set to $P(x[2])$, and the ϵ-checking process repeats. An example is shown in Fig. 27(b).

If $\|Px[2] - Px[1]\| < \epsilon$, then $Px[1]$ is accepted as the next point on $W^{u+}(x^*)$ (Fig. 27(c)). The $x[\ ]$ and $Px[\ ]$ arrays are both shifted one to the left (discarding $x[1]$ and $Px[1]$ in the process), $x[n_x]$ is set to $Px[1]$ (this keeps $x[n_x] = P(x[1])$), $Px[n_x]$ is set to $P(x[n_x])$, and then the ϵ-checking process is repeated.

The algorithm stops when a predetermined number of points has been output. Two examples of invariant manifolds—calculated using this algorithm—are shown in Fig. 28.

Comments:

i) The algorithm is initialized by setting n_x to 2, $x[1]$ to $x^* + \alpha\eta_1$, $x[2]$ and $Px[1]$ to $P(x[1])$, and $Px[2]$ to $P(x[2])$.

ii) The accuracy of the algorithm depends on the interpolation. The simple linear interpolation used here is accurate only if the portion of $W^{u+}(x^*)$ connecting $x[1]$ and $x[2]$ is nearly straight. This is the case at initialization since α is chosen such that $x[1]$ and $x[2]$ lie on η_1. It is true for the rest of the algorithm if ϵ is small (how small is problem-dependent).

iii) The $x[\ ]$ array increases in size, but never decreases. A scheme for decreasing the resolution automatically is helpful in some cases (e.g., when $W^{u+}(x^*)$ approaches a stable equilibrium point) and is discussed fully in [1].

iv) It is not necessary to calculate every value in the $Px[\ ]$ array; only the first two entries are ever used. However, during interpolation, $x[2]$ becomes $x[3]$, and $Px[2]$ should be saved in $Px[3]$ to avoid recalculation. Thus $Px[\ ]$ expands during an interpolation and shortens upon acceptance of $Px[1]$. n_{Px} is the number of elements in the $Px[\ ]$ array.

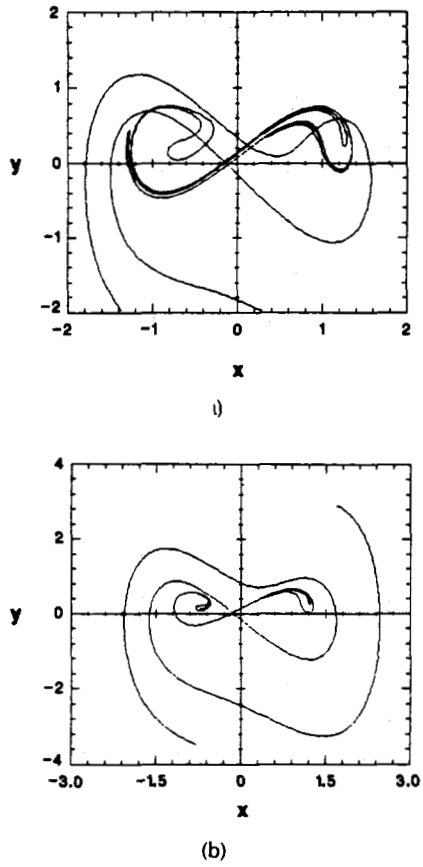

Fig. 28. Invariant manifolds of Duffing's equation. (a) Intersecting manifolds: $\delta = 0.25$, $\gamma = 0.3$, $\omega = 1.0$. (b) Nonintersecting manifolds: $\delta = 0.45$, $\gamma = 0.3$, $\omega = 1.0$

v) Calculation of the unstable manifold can be sensitive to the choice of ϵ, α, and the integration tolerance. The question of how long the algorithm can run before its output becomes unreliable is a difficult one. In practice, we run a simulation for given values of ϵ, α, and integration tolerance and then run the same simulation with tighter tolerances. The portion of the manifold where the two simulations agree is then known to be reliable.

vi) An unstable half-manifold of a saddle point may approach a stable equilibrium point. Control logic can be included in the algorithm to test whether the output points are accumulating at a point and, when they are, the Newton–Raphson algorithm can be used to test for the existence of a nearby equilibrium point.

vii) Each point of a period-K closed orbit $\{x_1^*, \cdots, x_K^*\}$ is a fixed point of the K-iterated map P^K. This algorithm can be modified to calculate all K of the $W^{u+}(x_k^*)$ simultaneously. See [1] for details.

XII. Calculation of Lyapunov Exponents

There is currently no method available for calculating all the Lyapunov exponents from data obtained via experiments though techniques exist for calculating the one or two largest positive exponents from an experimental time series [24]. In this section, we present an algorithm that cal-

culates all the Lyapunov exponents via computer simulations [25].

As a convenience to the reader, we restate the definition of Lyapunov exponents:

$$\lambda_i := \lim_{t \to \infty} \frac{1}{t} \ln |m_i(t)|, \qquad i = 1, \cdots, n \tag{36}$$

where the $m_i(t)$ are the eigenvalues of $\Phi_t(x_0, t_0)$.

The obvious way to find the Lyapunov exponents is to integrate $\Phi_t(x_0, t_0)$ for T seconds. The $m_i(t)$ can be found using EISPACK and, if T is large enough

$$\lambda_i \approx \frac{1}{T} \ln |m_i(T)|. \tag{72}$$

There are two problems with this approach. First, in a chaotic system, $\lambda_1 > 0$ and $\Phi_t(x_0, t_0)$ is unbounded as $t \to \infty$. Second, as $t \to \infty$, each column of $\Phi_t(x_0, t_0)$ tends to line up with the eigenvector associated with the largest eigenvalue $m_1(t)$. It follows that $\Phi_t(x_0, t_0)$ is ill-conditioned and its eigenvalues cannot be reliably computed.

A more robust algorithm is based on the following concept: almost every vector in the linearized system (32) evolves on the average as $e^{\lambda_1 t}$. Thus to find λ_1, choose a time interval $T > 0$, an iteration count K, and any initial condition $u^{(0)}$ normalized to 1. Calculate the solution to (32) for $t = KT$ normalizing every T seconds as follows:[32]

$$x^{(k)} = \delta x(kT; u^{(k-1)}, (k-1)T) \tag{73a}$$

$$u^{(k)} = x^{(k)} / \|x^{(k)}\| \tag{73b}$$

for $k = 1, \cdots, K$ where $\delta x(t; u, \tau) = \Phi_{t-\tau}(\phi_\tau(x_0, 0), \tau)u$ is the solution to (32) at time t starting from initial condition u at time τ. Then

$$\delta x(kT; u^{(0)}, 0) = \|x^{(1)}\| \cdots \|x^{(K)}\| u^{(K)} \tag{74}$$

and for K large enough

$$\lambda_1 \approx \frac{1}{KT} \ln \|\delta x(kT; u^{(0)}, 0)\| \tag{75a}$$

$$= \frac{1}{KT} \ln \prod_{k=1}^{K} \|x^{(k)}\| \tag{75b}$$

$$= \frac{1}{KT} \sum_{k=1}^{K} \ln \|x^{(k)}\|. \tag{75c}$$

Likewise, the *area* spanned by almost any two linearly independent vectors evolves in the linearized system (32) on the average as $e^{(\lambda_1 + \lambda_2)t}$. Hence, $\lambda_1 + \lambda_2$ can be found by following the time evolution of almost any two linear independent vectors x_1 and x_2. However, there is one previously mentioned complication: as x_1 and x_2 evolve, they tend to point in the same direction. This effect can be avoided by orthogonalizing as well as normalizing every T seconds. If modified Gram–Schmidt orthonormalization [26] is used, the formulas at the kth step are

$$x_1^{(k)} = \delta x(kT; u_1^{(k-1)}, (k-1)T) \tag{76a}$$

$$x_2^{(k)} = \delta x(kT; u_2^{(k-1)}, (k-1)T) \tag{76b}$$

$$v_1^{(k)} = x_1^{(k)} \tag{76c}$$

$$u_1^{(k)} = v_1^{(k)} / \|v_1^{(k)}\| \tag{76d}$$

$$v_2^{(k)} = x_2^{(k)} - \langle x_2^{(k)}, u_1^{(k)} \rangle u_1^{(k)} \tag{76e}$$

$$u_2^{(k)} = v_2^{(k)} / \|v_2^{(k)}\| \tag{76f}$$

where $\langle \cdot, \cdot \rangle$ denotes the inner product $\langle x, y \rangle := x^T y$.

$u_1^{(0)}$ and $u_2^{(0)}$ are almost any orthonormal pair of vectors. $u_1^{(k)}$ and $u_2^{(k)}$ are the normalized versions of $v_1^{(k)}$ and $v_2^{(k)}$ which are the orthogonalized versions of $x_1^{(k)}$ and $x_2^{(k)}$. It is important in this method that the same two-dimensional subspace is followed at each step, that is, $\{x_1^{(k)}, x_2^{(k)}\}$ and $\{u_1^{(k)}, u_2^{(k)}\}$ must span the same subspace. Fortunately, this requirement is satisfied by the modified Gram–Schmidt orthonormalization procedure.

At each step in the iteration, the area is given by $\|v_1^{(k)}\| \|v_2^{(k)}\|$ so, for K large,

$$\lambda_1 + \lambda_2 \approx \frac{1}{KT} \sum_{k=1}^{K} \ln \|v_1^{(k)}\| \|v_2^{(k)}\| \tag{77a}$$

$$= \frac{1}{KT} \sum_{k=1}^{K} \ln \|v_1^{(k)}\| + \frac{1}{KT} \sum_{k=1}^{K} \ln \|v_2^{(k)}\| \tag{77b}$$

$$= \lambda_1 + \frac{1}{KT} \sum_{k=1}^{K} \ln \|v_2^{(k)}\| \tag{77c}$$

and, therefore,

$$\lambda_2 \approx \frac{1}{KT} \sum_{k=1}^{K} \ln \|v_2^{(k)}\|. \tag{78}$$

In general, almost every k-dimensional volume element evolves on the average as $e^{(\lambda_1 + \cdots + \lambda_k)t}$. By following the evolution of volume elements with dimensions from 1 to n, one can calculate each of the Lyapunov exponents.

Pseudo-code for calculating all n Lyapunov exponents simultaneously is shown in Fig. 29. At each iteration, the

```
begin LyapunovExponent
    choose T, E_r, E_a, k_max
    choose matrix u[][] with orthonormal columns
    for i from 1 to n
        set sum[i] = 0
        set λ[i] = 0
    set k = 0
    repeat
        set k = k + 1
        if k = k_max then
            no convergence—exit
        set λ_old[] = λ[]
        integrate variational equation from u[][]
        put the result in matrix x[][]
        for i from 1 to n
            set v[][i] = x[][i]
            for j from 1 to i − 1
                set v[][i] = v[][i] − <v[][i], u[][j]> u[][j]
            set u[][i] = v[][i]/||v[][i]||
            set sum[i] = sum[i] + ln ||v[][i]||
            set λ[i] = sum[i]/kT
    until k > 1 and ||λ_old[] − λ[]|| < E_r||λ[]|| + E_a
    output λ[]
end LyapunovExponent
```

Fig. 29. Pseudo-code for the calculation of the Lyapunov exponents. Double brackets indicate a variable is a matrix (i.e., a two-dimensional array). An index in the second pair of brackets indicates a column vector (e.g., $v[\,][i]$ is the ith column of $v[\,][\,]$).

matrix-valued variational equation (31) is integrated from the initial condition $[u_1^{(k-1)} \cdots u_n^{(k-1)}]$ for T seconds to get $[x_1^{(k)} \cdots x_n^{(k)}]$ which is then orthogonalized to obtain $[v_1^{(k)} \cdots v_n^{(k)}]$ which is normalized to get $[u_1^{(k)} \cdots u_n^{(k)}]$. This process is repeated until the Lyapunov exponents converge or a

[32] We assume $t_0 = 0$ for simplicity.

maximum number of iterations is reached. By analogy with the result presented for λ_2, it can be shown that, for K large enough,

$$\lambda_i \approx \frac{1}{KT} \sum_{k=1}^{K} \ln \|v_i^{(k)}\|, \qquad i = 1, \cdots, n. \tag{79}$$

One question remains: How is T chosen? T should be picked small enough to guarantee that the numerical limitations of the computer are not approached with respect to overflow and ill-conditioning of $[x_1^{(k)} \cdots x_i^{(k)}]$, but not so small that the algorithm becomes inefficient due to excessive orthonormalization. Typically T is chosen on the order of the natural period of the system.

XIII. Calculation of Dimension

The numerical calculation of dimension is an active research topic and as of yet there is no best way to compute any of the dimensions. All the techniques discussed here attempt to estimate dimension using a single uniformly sampled trajectory of dimension n. The data can be obtained via simulation or experiment and can be either an actual or reconstructed trajectory.

A. Capacity

The first attempts to calculate capacity were based directly on the definition. Cover the state space with a grid of boxes (hyper-cubes) of side ϵ. $N(\epsilon)$ is calculated by counting the number of boxes in which data points lie. From (38)

$$\ln N(\epsilon) = D_{\text{cap}} \ln \frac{1}{\epsilon} + \ln k. \tag{80}$$

Hence, D_{cap} is the slope of a log-log plot of $N(\epsilon)$ versus $1/\epsilon$. This ϵ-grid technique works, but has two drawbacks:

i) For systems of dimension greater than three, the memory requirements of the ϵ-grid are excessive.

ii) A large amount of data is required to ensure that nearly every box that contains a point on the attractor is visited by the trajectory under study; otherwise, the estimate of D_{cap} will be low.

A more efficient algorithm is based on the relationship [27]

$$D_{\text{cap}} = n - \lim_{\epsilon \to 0} \frac{\ln V(\epsilon)}{\ln \epsilon}. \tag{81}$$

where $V(\epsilon) :=$ volume $\{x \in \mathbb{R}^n \mid \text{dist}(x, A) < \epsilon\}$ is the volume of the set of all points in an ϵ-neighborhood of the attractor A. $V(\epsilon)$ can be found efficiently using Monte Carlo techniques and the second term of the right-hand side of (81) can be approximated by the slope of the log-log plot of $V(\epsilon)$ versus ϵ. The interested reader is referred to [28] for more details.

B. Information Dimension

As with capacity, the first attempts to calculate information dimension used an ϵ-grid. P_i is approximated by n_i/N where n_i is the number of data points in the ith box and N is the total number of data points. D_I is estimated by the slope of a log-log plot of

$$-\sum_{i=1}^{N} P_i \ln P_i$$

versus $1/\epsilon$.

This approach suffers from the same disadvantages as it does when applied to capacity, though the probabilistic nature of D_I lessens the amount of data required for an accurate estimation.

More robust algorithms utilize nearest neighbor techniques [29] as well as projection pursuit techniques [30]. The interest reader is referred to these papers as well as [31] for more information on the computation of information dimension.

C. Correlation Dimension

Correlation dimension may be calculated directly from the definition using an ϵ-grid, but it is more efficient and robust to use the correlation as defined in (44)

$$C(\epsilon) := \lim_{N \to \infty} \frac{1}{N^2} \{\text{the number of pairs of points } x_i, x_j \text{ such that } \|x_i - x_j\| < \epsilon\} \tag{44}$$

where N is the total number of data points.

For a given ϵ, the estimation of $C(\epsilon)$ entails computing all the distances $d_{ij} := \|x_i - x_j\|$ and counting the number $N_d(\epsilon)$ of $d_{ij} < \epsilon$ for $i, j = 1, \cdots, N$. Then $C(\epsilon) \approx N_d(\epsilon)/N^2$.

The d_{ij} can be computed efficiently by taking advantage of the floating-point representation used in computers. A floating-point number d_{ij} is represented by a sequence of bits using a mantissa/exponent format

$$d_{ij} = \pm m b^e \tag{82}$$

where the exponent e is an integer, the base b is also an integer, typically some power of two, and the mantissa m is a fraction with $1/b < m \leq 1$. For example, in the 32-bit IEEE standard, the base is 2, the first bit stores the sign information, the next eight bits hold the exponent, and the remaining 23 bits represent the mantissa. Using shifting and masking functions, the exponent can be retrieved without any time-consuming floating-point operations.

To take advantage of this representation, choose ϵ as a power of two, $\epsilon = 2^p$. Then $d_{ij} < \epsilon$ if and only if $e \leq p$. Thus $N_d(\epsilon)$ can be calculated for logarithmically spaced values of ϵ (which is just what is needed) by creating an integer array ***Nd***[ ] initialized to all zeros. As each d_{ij} is calculated, increment ***Nd***[e] by one where e is the exponent obtained directly from the binary representation of d_{ij}. When all the d_{ij} have been calculated

$$N_d(2^p) = \sum_{i=1}^{p} \textbf{\textit{Nd}}[i]. \tag{83}$$

Pseudo-code for the complete algorithm is shown in Fig. 30.

Comments:

i) The exponent e may be negative and cannot be used directly as an index to the ***Nd***[ ] array. Instead, a constant offset or bias is added to e to guarantee the index is positive. In the IEEE floating-point standard, the exponent is already stored with an offset added to it. This offset ensures that the stored value is never negative, but it could be 0; therefore, with programming languages that do not allow 0 as an index, 1 should be added to the biased version of the exponent.

ii) Owing to duplications, not all the inter-point distances need to be computed. Only the $N(N-1)$ values d_{ij} for $i = 1, \cdots, N$ and $j = i+1, \cdots, N$ need to be calculated.

```
begin CorrelationDimension
    set p_min = Nd_max
    set p_max = 1
    for i from 1 to Nd_max
        set Nd[i] = 0
    for i from 1 to N-1
        for j from i+1 to N
            set d = ||x[i] - x[j]||^2
            set e to the exponent of d
            set e = e + offset
            set Nd[e] = Nd[e] + 1
            if e < p_min then
                set p_min = e
            if e > p_max then
                set p_max = e
    set sum = 0
    for p from p_min to p_max
        set sum = sum + Nd[i]
        plot x = p/2 versus y = ln(sum/(N(N-1))/ln 2
end CorrelationDimension
```

Fig. 30. Pseudo-code for the calculation of the correlation dimension.

iii) If N is very large, a subset $\{x_{i_1}, \cdots, x_{i_{n_{ref}}}\}$ of data points can be chosen as reference points where $n_{ref} < N$ and the indices $\{i_1, \cdots, i_{n_{ref}}\}$ are chosen at random from $[1, \cdots, N]$. The algorithm is unchanged except that the distances between each of the reference points and the other $N - n_{ref}$ points are calculated and used to update the $Nd[\ ]$ array.

iv) There will exist some p_{min} and p_{max} such that $Nd[p] = 0$ for $p < p_{min}$ and for $p > p_{max}$. Only values of p between p_{min} and p_{max} need to be plotted in the log-log graph.

v) To save the time it takes to perform a square root, $d_{ij}^2 = \|x_i - x_j\|^2$ is used instead of d_{ij}. This explains why $p/2$ is plotted on the x-axis instead of p.

vi) We are interested only in the slope of the log-lot plot so there is no need to unbias the exponent before plotting.

vii) D_C is the slope of the log-log plot and is calculated using a least-squares fit

$$\text{slope} = \frac{\sum_{i=1}^{N} x_i y_i - \sum_{i=1}^{N} y_i \sum_{i=1}^{N} x_i}{\sum_{i=1}^{N} x_i^2 - \left(\sum_{i=1}^{N} x_i\right)^2} \tag{84}$$

where the x_i correspond to $\ln \epsilon$ and the y_i correspond to $\ln C(\epsilon)$. A typical log-log plot is shown in Fig. 31(a). It is clear from the figure that there is a limited range where the slope is approximately constant and only data from this range should be used to estimate D_C. Unfortunately, there is currently no robust technique available to detect the useful range of ϵ automatically.

viii) In Section VII-C it was mentioned that x_i, x_i should be counted as a pair in $C(\epsilon)$. Theoretically, this is true but, in practice, x_i, x_i should not be counted. $d_{ii} = 0$ for $i = 1, \cdots, n$ implying that

$$\lim_{\epsilon \to 0} N_d(\epsilon)/N^2 = 1/N.$$

Thus for finite N, inclusion of the d_{ii} in $N_d(\epsilon)$ decreases the useful range of the log-log plot (Fig. 31(b)).

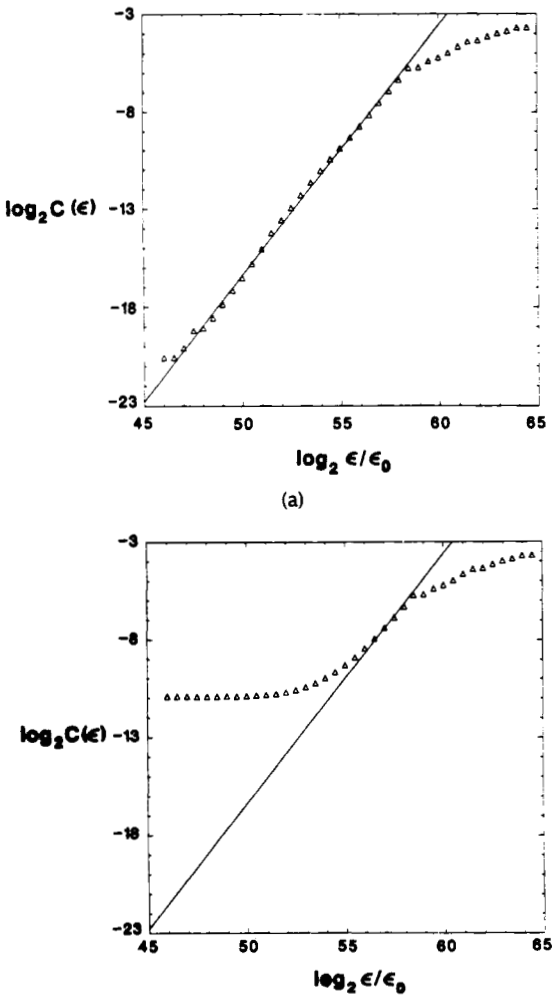

Fig. 31. $\log_2 C(\epsilon)$ versus $\log_2 \epsilon$ for Henon's map: $x_{k+1} = y_k + 1 - 1.4x_k^2$, $y_{k+1} = 0.3x_k$. ϵ_0 is a constant that accounts for the biasing of the exponent. It does not affect the slope. (a) The slope and, therefore, D_C is approximately 1.28. (b) Same as (a) except the d_{ii} are counted in $N_d(\epsilon)$ restricting the useful range of ϵ.

Acknowledgment

The authors would like to thank P. Kennedy and G. Bernstein for their helpful comments on the manuscript.

References

[1] T. S. Parker and L. O. Chua, *Practical Numerical Algorithms for Chaotic Systems.* New York, NY: Springer-Verlag, in progress.

[2] J.-P. Eckmann and D. Ruelle, "Ergodic theory of chaos and strange attractors," *Rev. Mod. Phys.*, vol. 57, no. 3, July 1985.

[3] M. W. Hirsch and S. Smale, *Differential Equations, Dynamical Systems, and Linear Algebra.* New York, NY: Academic Press, 1974.

[4] J. Milnor, "On the concept of attractor," *Commun. Math. Phys.*, vol. 99, pp. 177–195, 1985.

[5] M. Koksal, "On the state equations of nonlinear networks and the uniqueness of their solutions," *Proc. IEEE*, vol. 74, pp. 513–514, Mar. 1986.

[6] B. B. Mandelbrot, *Fractals: Form, Chance and Dimension.* San Francisco, CA: Freeman, 1977.

[7] J. Guckenheimer and P. Holmes, *Nonlinear Oscillations, Dynamical Systems and Bifurcations of Vector Fields.* New York, NY: Springer-Verlag, 1983, pp. 230–235.

[8] C. A. Desoer, *Notes for a Second Course on Linear Systems.* New York, NY: van Nostrand Reinhold, 1970.

[9] L. O. Chua, C. A. Desoer, and E. S. Kuh, *Linear and Nonlinear Circuits.* New York, NY: McGraw-Hill, 1987.

[10] H. Haken, "At least one Lyapunov exponent vanishes if the trajectory of an attractor does not contain a fixed point," *Phys. Lett.*, vol. 94A, no. 2, pp. 71–72, Feb. 1983.

[11] O. E. Rossler, "An equation for hyperchaos," *Phys. Lett.*, vol. 71A, p. 155, 1979.

[12] L. S. Young, "Entropy, Lyapunov exponents, and Hausdorff dimension in differentiable dynamic systems," *IEEE Trans. Circuits Syst.*, vol. CAS-30, no. 8, pp. 599-607, Aug. 1983.
[13] P. Frederickson, J. L. Kaplan, E. D. Yorke, and J. A. Yorke, "The Liapunov dimension of strange attractors," *J. Diff. Eq.*, vol. 49, pp. 185-207, 1983.
[14] P. Grassberger and I. Procaccia, "Measuring the strangeness of strange attractors," *Physica 9D*, pp. 189-208, 1983.
[15] F. Takens, "Detecting strange attractors in turbulence," in *Warwick 1980 Lecture Notes in Math.*, vol. 898. Berlin, W. Germany: Springer, pp. 366-381.
[16] T. S. Parker and L. O. Chua, "INSITE—A software toolkit for the analysis of nonlinear systems," this issue, pp. 1081-1089.
[17] J. J. Dongarra, C. B. Moler, J. R. Bunch, and G. W. Stewart, *LINPACK Users' Guide*. Philadelphia, PA: SIAM, 1979.
[18] L. O. Chua and P.-M. Lin, *Computer-Aided Analysis of Electronic Circuits: Algorithms and Computational Techniques*. Englewood Cliffs, NJ: Prentice-Hall, 1975.
[19] B. T. Smith, J. M. Boyle, J. J. Dongarra, B. S. Garbow, Y. Ikebe, V. C. Klema, and C. B. Moler, "Matrix eigensystem routines—EISPACK guide, second edition," in *Lecture Notes in Computer Science*. New York, NY: Springer-Verlag, 1976.
[20] T. J. Aprille and T. N. Trick, "A computer algorithm to determine the steady-state response of nonlinear oscillators," *IEEE Trans. Circuits Syst.*, vol. CAS-4, pp. 354-360, July 1972.
[21] A. I. Mees, *Dynamics of Feedback Systems*. New York, NY: Wiley, 1981, pp. 126-128.
[22] I. G. Kevrekidis, R. Aris, L. D. Schmidt, and S. Pelikan, "Numerical computation of invariant circles of maps," *Physica 16D*, pp. 243-251, 1985.
[23] A. Ushida and L. O. Chua, "Frequency-domain analysis of nonlinear circuits driven by multi-tone signals," *IEEE Trans. Circuits Syst.*, vol. CAS-31, no. 9, pp. 766-779, Sept. 1984.
[24] A. Wolf, J. B. Swift, H. L. Swinney, and J. A. Vastano, "Determining Lyapunov exponents from a time series," *Physica 16D*, pp. 285-317, 1985.
[25] I. Shimada and T. Nagashima, "A numerical approach to ergodic problem of dissipative dynamical systems," *Prog. Theor. Phys.*, vol. 61, no. 6, pp. 1605-1616, June 1979.
[26] B. Noble and J. W. Daniel, *Applied Linear Algebra, second edition*. Englewood Cliffs, NJ: Prentice-Hall, 1977.
[27] E. Ott, E. D. Yorke, and J. A. Yorke, "A scaling law: How an attractor's volume depends on noise level," *Physica 16D*, pp. 62-78, 1985.
[28] F. Hunt and F. Sullivan, "Efficient algorithms for computing fractal dimensions," in *Dimensions and Entropies in Chaotic Systems*, G. Mayer-Kress, Ed. New York, NY: Springer-Verlag, 1986.
[29] K. W. Pettis, T. A. Bailey, A. K. Jain, and R. C. Dubes, "An intrinsic dimensionality estimator from near-neighbor information," *IEEE Trans. Pattern Anal. Machine Intell.*, vol. PAMI-1, no. 1, pp. 25-37, Jan. 1979.
[30] P. J. Huber, "Projection pursuit," *Ann. Statist.*, vol. 13, pp. 435-475, 1985.
[31] R. L. Somorjai, "Methods for estimating the intrinsic dimensionality of high-dimensional point sets," in *Dimensions and Entropies in Chaotic Systems*, G. Mayer-Kress, Ed. New York, NY: Springer-Verlag, 1986.

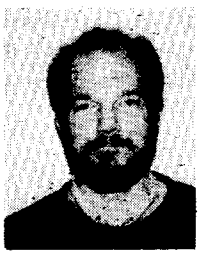

Thomas S. Parker was born in Pasadena, CA, on November 21, 1957. He received the B.S. (with highest honors) and M.S. degrees in electrical engineering from the University of California at Berkeley in 1980 and 1982, respectively. He was a Hertz Fellow from 1981 to 1986 and received the Ph.D. degree from U.C. Berkeley in May 1987.

His research interests encompass nonlinear dynamical systems, numerical methods, and strange behavior.

Leon O. Chua (Fellow, IEEE), for a photograph and biography, please see page 980 of this issue.

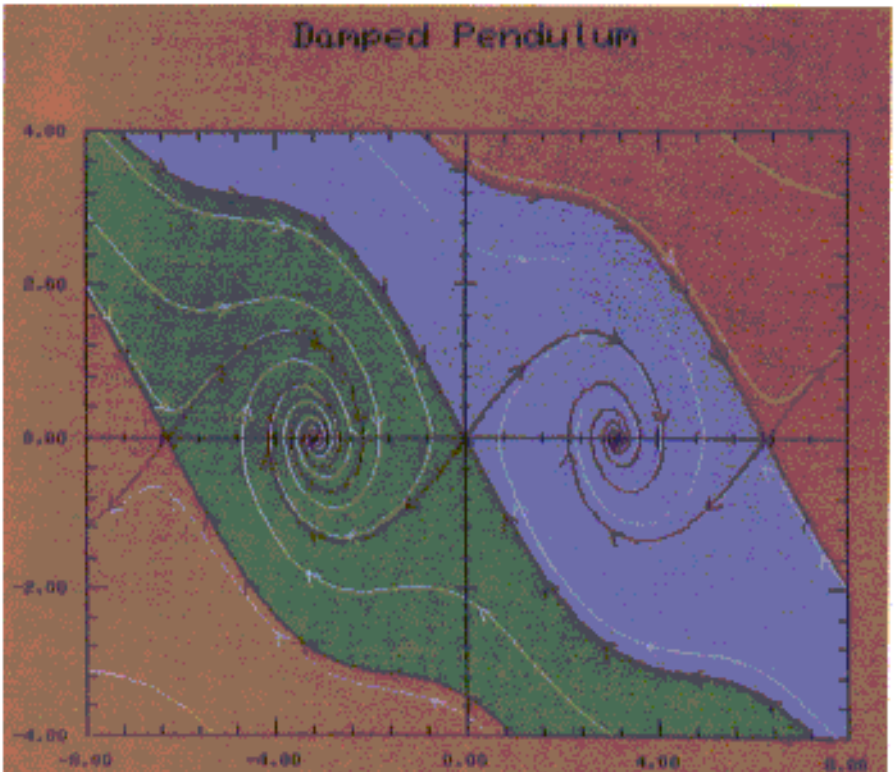

Fig. 1. Phase portrait of the pendulum equation. The white trajectories have been randomly chosen to indicate typical behavior of the system. There are two stable equilibria at $(\pm\pi, 0)$ and three saddle points at $(0, 0)$ and $(\pm 2\pi, 0)$. Each red trajectory tends toward one of the saddle points as $t \to \infty$ or as $t \to -\infty$. Each of the two shaded regions indicates the basin of attraction of one of the stable equilibria. Note that the red trajectories that approach the saddle points as $t \to \infty$ are the boundaries of the basins of attraction.